ΕΘΝΙΚΟ ΜΕΤΣΟΒΙΟ ΠΟΛΥΤΕΧΝΕΙΟ
ΣΧΟΛΗ ΗΛΕΚΤΡΟΛΟΓΩΝ ΜΗΧΑΝΙΚΩΝ
ΚΑΙ ΜΗΧΑΝΙΚΩΝ ΥΠΟΛΟΓΙΣΤΩΝ
ΤΟΜΕΑΣ ΗΛΕΚΤΡΙΚΗΣ ΙΣΧΥΟΣ

Θερμιδομετρική διάταξη για την μέτρηση απωλειών ισχύος σε μετατροπείς Silicon Carbide

ΔΙΠΛΩΜΑΤΙΚΗ ΕΡΓΑΣΙΑ

Γεώργιος Ε. Σφακιανάκης

Επιβλέπων : Στέφανος Ν. Μανιάς
Καθηγητής Ε.Μ.Π.

Αθήνα, Μάιος 2013

ΕΘΝΙΚΟ ΜΕΤΣΟΒΙΟ ΠΟΛΥΤΕΧΝΕΙΟ
ΣΧΟΛΗ ΗΛΕΚΤΡΟΛΟΓΩΝ ΜΗΧΑΝΙΚΩΝ
ΚΑΙ ΜΗΧΑΝΙΚΩΝ ΥΠΟΛΟΓΙΣΤΩΝ
ΤΟΜΕΑΣ ΗΛΕΚΤΡΙΚΗΣ ΙΣΧΥΟΣ

Θερμιδομετρική διάταξη για την μέτρηση απωλειών ισχύος σε μετατροπείς Silicon Carbide

ΔΙΠΛΩΜΑΤΙΚΗ ΕΡΓΑΣΙΑ

Γεώργιος Ε. Σφακιανάκης

Επιβλέπων : Στέφανος Ν. Μανιάς
Καθηγητής Ε.Μ.Π.

Εγκρίθηκε από την τριμελή εξεταστική επιτροπή την 13η Μαΐου 2013.

.....	.....	.....
Στέφανος Μανιάς	Αντώνιος Κλαδάς	Σταύρος Παπαθανασίου
Καθηγητής Ε.Μ.Π.	Καθηγητής Ε.Μ.Π.	Επίκουρος Καθηγητής Ε.Μ.Π.

Αθήνα, Μάιος 2013

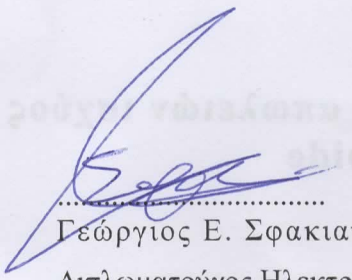

.....

Γεώργιος Ε. Σφακιανάκης

Διπλωματούχος Ηλεκτρολόγος Μηχανικός και Μηχανικός Υπολογιστών Ε.Μ.Π.

Περιληψη

Ο σχεδιασμός μετατροπέων ισχύος με ημιαγωγούς απο καρβίδιο πυριτίου (SiC) μπορεί να ακολουθήσει τρείς κατευθύνσεις. Αυτές είναι η υψηλή διακοπτική συχνότητα, η υψηλή θερμοκρασία και η υψηλή απόδοση. Η υψηλή απόδοση προτιμάται για μετατροπείς με ονομαστικές ισχύς, από δεκάδες W μέχρι και κάποια MW. Συγκεκριμένα, οι αναμενόμενες αποδόσεις για τέτοιους μετατροπείς ισχύος, είναι πάνω από 99.5%. Επομένως, οι αναμενόμενες απώλειες ισχύος είναι πολύ χαμηλές σε σχέση με την ονομαστική ισχύ και η μέτρηση τους αντιμετωπίζει προβλήματα τα οποία πρέπει να αντιμετωπισθούν.

Οι τυπικές μέθοδοι μέτρησης της απόδοσης βασίζονται στην μέτρηση των ισχύων εισόδου και εξόδου. Ωστόσο, η μέτρηση αυτή περιέχει μεγάλα σφάλματα τα οποία οφείλονται στα σφάλματα ανάγνωσης της τάσης και του ρεύματος καθώς και στα σφάλματα ανάγνωσης της διαφοράς φάσης των δύο μεγεθών. Η ηλεκτρομαγνητική παρενόχληση (EMI) μπορεί επίσης να δημιουργήσει προβλήματα στην ανάγνωση αυτών των μεγεθών. Οι μετρούμενες ποσότητες, περιέχουν αρμονικές υψηλής τάξης τις οποίες τα περισσότερα ψηφιακά όργανα δεν είναι σε θέση να μετρήσουν με υψηλή ακρίβεια. Συνεπώς, είναι δύσκολο να μετρηθεί με ακρίβεια η απόδοση τέτοιων μετατροπέων των οποίων η απόδοση υπερβαίνει το 99.5%.

Ως εκ τούτου, είναι απαραίτητο να χρησιμοποιηθεί μια άμεση μέθοδος, για να μετρηθούν με ακρίβεια οι απώλειες ισχύος. Μια θερμιδομετρική διάταξη είναι σε θέση να μετρήσει με ακρίβεια την θερμότητα που εκλύεται από έναν μετατροπέα, δηλαδή να μετρήσει άμεσα τις απώλειες ισχύος, με ένα σφάλμα που κυμαίνεται από 5% έως και 1%.

Σε αυτή την διπλωματική εργασία, παρουσιάζεται η διαδικασία σχεδιασμού και υλοποίησης μιας θερμιδομετρικής διάταξης ανοιχτού τύπου, για τη μέτρηση απωλειών ισχύος, για μετατροπείς πυριτίου καρβιδίου. Παρουσιάζεται αναλυτικά η διαδικασία σχεδιασμού, καθώς δίνεται και το απαιτούμενο θεωρητικό υπόβαθρο. Υπάρχει μια εκτεταμένη ανάλυση αυτού, καθώς και πως αυτό συνεισφέρει στην πορεία αυτής της διπλωματικής εργασίας. Έπειτα, παρουσιάζονται η διαστασιολόγηση του συστήματος , η υλοποίηση, η κατασκευή του, καθώς επίσης αναφέρονται και οι πιθανές πηγές σφαλμάτων της μέτρησης. Επιπρόσθετα, περιγράφεται ο τρόπος με τον οποίο έγινε η βαθμονόμηση και παραθέτονται οι σχετικές μετρήσεις. Στην θερμιδομετρική διάταξη τοποθετείται και μετράται η απόδοση ενός dc/dc μετατροπέα ανύψωσης τάσης, ο οποίος αποτελείται από 4 ημιαγωγούς SiC (BJT) σε παράλληλη σύνδεση. Δίνονται πειραματικά αποτελέσματα τα οποία συγκρίνονται με τα αποτελέσματα που λαμβάνονται χρησιμοποιώντας ένα μετρητή ισχύος και τέλος, δίνονται προτάσεις για εξέλιξη της παρούσας εργασίας καθώς και μια ανάλυση των κύριων συμπερασμάτων της εργασίας.

Λέξεις κλειδιά: Θερμιδομετρική διάταξη, Απώλειες ισχύος, Ημιαγωγοί πυριτίου-καρβιδίου, μετατροπείς ισχύος, Labview, Matlab

Abstract

Three design directions might be used when silicon carbide power semiconductor devices are employed in power electronics converters. High switching frequency, high-temperature operation and high efficiency count as these three directions. The last design direction is favorable in power electronics converters having power ratings from a few tens of W up to several hundreds of MW. In particular, efficiencies well above 99.5% are expected for silicon carbide converters. The anticipated power losses is, therefore, very low and, thus, issues related to accurately measure this low amount of power losses must be dealt with.

The typical measurement way of efficiencies is based on measuring the inlet and outlet powers. However, this results in huge errors due to reading errors of the voltage and current as such, but also due the phase-angle between the voltage and current. Electromagnetic interference (EMI) might also cause reading errors of the important quantities. The measurement quantities contain high order terms and most of the digital instruments are unable to measure them with high accuracy. Consequently, it is a difficult task to accurately measure the efficiency of such converters which might have efficiencies exceeding 99.5%.

Therefore, it is necessary to use a direct method in order to accurately measure the power losses. A calorimetric power loss measurement setup is able to measure the heat dissipated from a device and as a result to measure directly the power losses with a negligible error which may vary from 5% to even 1%.

In this thesis, the design process and implementation of an open type calorimetric power loss measurement setup for silicon carbide power electronics converters is presented. The design process is analytically presented and a theoretical background is also given. There is an extended analysis of the theoretical background presented and how this background fits to the project requirements. Afterwards, the dimensioning of the system and the implementation process are presented while possible sources of errors are also discussed. Furthermore, the way that the measurement setup has been calibrated is analyzed and related experimental results are shown. The efficiency of a 6 kW dc/dc boost converter consisting of 4 parallel-connected silicon carbide bipolar junction transistors was measured using the calorimetric setup. Various experimental results are shown and compared to results obtained using a power meter. A discussion along with suggestions for future work are given in the last chapter.

Keywords: Calorimetric Setup, Power losses, Silicon Carbide (SiC), Converters, LabView, Matlab

Acknowledgments

The present thesis was carried out during the fall semester of 2012-2013 at the Electrical Energy Conversion(E2C) laboratory of Kungliga Tekniska Hogskolan (KTH), Sweden. Hoping not to forget anyone, I would like to thank:

Dimosthenis Peftitsis for his support during this work and for reviewing this manuscript. Along with Dimosthenis I would also like to thank Jacek Rabkowski for their contribution during the measurements.

My Professor Stefanos Manias for giving me the chance to work on my master thesis abroad. Also I would like to thank my professors Stefanos Manias, Antonios Kladas and Stavros Papathanassiou for the inspiration to occupy with electric power and power electronics.

My Professors Staffan Norrga and Hans-Peter Nee for providing me with technical knowledge and continuous encouragement throughout the project.

All the people at E2C laboratory for their hospitality and especially Jesper for his support at the construction part of this project.

Haris Patsios for his advices before and during my thesis work.

Konstantinos Pavlou for encouraging me to work on my master thesis in Sweden.

Ioannis Chatzis for having great time the last 8 months in Stockholm and Antonios Antonopoulos for the discussions we had for several issues.

My family for their continuous support all these years. Last but not least I would like to thank Maria and all my friends for their support.

Georgios Sfakianakis
Stockholm, May 2013

Contents

List of Figures

List of Tables

Chapter 1

Introduction

Silicon carbide semiconductors allow the design and implementation of several power electronics converters which operate at very high temperatures, at high switching frequencies and the last but not least with a very high efficiency. Because of the continuous increase of silicon carbide power converters efficiency, which may exceed 99.5% [4], the accurate measurement of the efficiency of these converters is getting harder. Typical measurement ways of inlet and outlet power contain a huge error [2] [5] due to reading errors of voltage-current phase angle and electromagnetic interference (EMI). Furthermore, the measured quantities contain high order terms and most of the digital instruments are unable to accurately measure the inlet and outlet power. Consequently, it is not a trivial issue to accurately measure the efficiency of such devices.

1.1 Purpose

This thesis is about the design and implementation of a calorimetric power loss measurement setup for SiC power converters. A calorimetric power loss measurement setup is able to measure the heat dissipated from the device without involving current and voltage measurements and having a negligible error of 1% – 5%. This count as the main advantage in comparison to electrical indirect methods. Such equipment is necessary at modern laboratories in order to contribute in the research performed in the field of SiC power electronics and industrial electronics in general.

1.2 Main scientific contributions of the thesis

The main scientific contributions of the thesis are the following:

- Implementation of a fully-automated control and measurement system.
- Development of an accurate measurement tool for very high-efficiency SiC converters.
- Investigation of the various error contributions associated with open-type calorimeters

- Various ways in order to improve the overall accuracy of the systems are also shown.

1.3 Outline of the Thesis

This thesis contain a full presentation of the theoretical study, design, implementation and optimization of the calorimetric setup.

- *Chapter 2* provides the overview of general principles of heat transfer theory along with engineering formulas.
- *Chapter 3* introduces the theoretical background. Silicon carbide semiconductor and converters, overview of measurements, calorimeter theory and error propagation theory are the topics which are extensively discussed.
- *Chapter 4* presents the design and implementation process. The reason why open type calorimeter is chosen, the background for this construction, and the dimensioning are presented. Moreover, there is a full discussion about the reasons of inaccuracy, the selection of the equipment and the theoretical accuracy in the measurements.
- *Chapter 5* shows the the calibration process of the setup. Furthermore, measurement tests are applied at a dc/dc converter built with SiC semiconductors. The obtained results are discussed.
- *Chapter 6* summarizes the present work and outlines future work guidelines.

Chapter 2

Heat Transfer Theory

A temperature difference that exists within a system or two brought into contact systems , causes transfer of energy. This process of energy transportation is recognized as heat transfer. Three different ways of heat transmission can be distinguished: conduction , convection and radiation. General principles of heat transfer theory are presented in the this section.

2.1 Conduction

Conduction is a mode of heat transfer by which heat flows through a solid. the basic principle of heat conduction was proposed by the French scientist J.Fourier in 1822 and is worldwide knows as *Fourier's law*. For a one-dimensional plane geometry, this statement is expressed as [6]

$$q_k = -\kappa A \frac{dT}{dx} \tag{2.1}$$

where q_k is the rate of heat transfer(i.e. power) by conduction through the surface of a plate with are A as shown in Fig. 2.1 , $dT = t_1 - t_2$ is temperature difference and dx is the distance between the walls of the plate. The constant of proportionality k is the thermal conductivity of the material the plate is made of. The value of k for different materials varies from 0.026 $W/(m \cdot K)$ for air to 427 $W/(m \cdot K)$ for silver[7].The thermal conductivity can also be anisotropic, in which case k is a matrix.

The negative sign in Equation 2.1 is introduced as the result of the convection that the heat flow rate is taken to be positive in the direction of a decreasing temperature.

However, Equation 2.1 does not account for all energy, but only for the energy injected into a plate . To obtain the differential conduction Equation, the principle of conservation of energy should be applied. Derivation of the equation can be found in different literature [6, 8] and is therefore not treated here. The derived equation for one-dimensional heat transfer by means of conduction is given by [6]

$$k \frac{\vartheta^2 T}{\vartheta x^2} + q^*_G = \rho c \frac{\vartheta T}{\vartheta t} \tag{2.2}$$

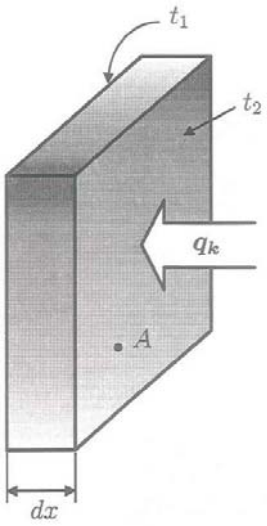

Figure 2.1: Fourier's law of conduction applied for a one-dimensional plane geometry.

where ρ is the density and c is the thermal capacity (or specific heat capacity) of the material. The first term on left side represents the net rate of heat flow into certain volume. The second term on the left side is the rate of energy per unit volume produced inside of the volume. The right side represents the rate of change in internal energy inside of the volume. The derivation of Eq. 2.2 was based on the assumption that the temperature distribution is one-dimensional. If this constraint is removed, temperature becomes dependent on all three-dimensional control volume in Fig. 2.2 is expressed as [6]

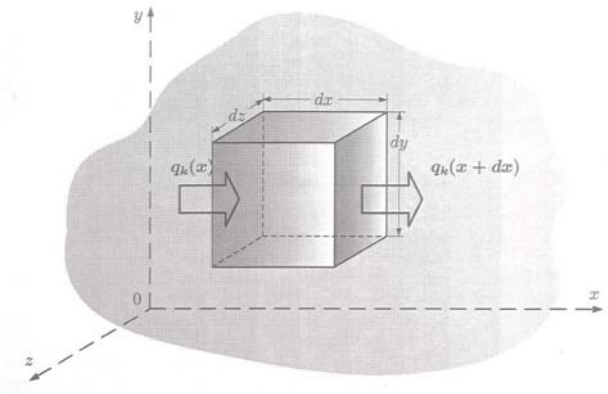

Figure 2.2: Control volume for three-dimensional conduction

$$\frac{\vartheta^2 T}{\vartheta x^2} + \frac{\vartheta^2 T}{\vartheta y^2} + \frac{\vartheta^2 T}{\vartheta z^2} + \frac{q_G^*}{k} = \frac{1}{\alpha}\frac{\vartheta T}{\vartheta t} \tag{2.3}$$

where α is the thermal diffusivity, defined as

$$\alpha = \frac{k}{\rho c} \tag{2.4}$$

For stationary problem, the temperature of a material is not time dependent, i.e. $T = T(x, y, z)$, and the right term can therefore be ignored. The steady-state form of the three-dimensional heat conduction equation is

$$\frac{\vartheta^2 T}{\vartheta x^2} + \frac{\vartheta^2 T}{\vartheta y^2} + \frac{\vartheta^2 T}{\vartheta z^2} + \frac{q_G^*}{k} = 0 \tag{2.5}$$

If the system is under stationary conditions and no heat is generated internally, the conduction equation has the form of

$$\frac{\vartheta^2 T}{\vartheta x^2} + \frac{\vartheta^2 T}{\vartheta y^2} + \frac{\vartheta^2 T}{\vartheta z^2} = 0 \tag{2.6}$$

Eq. 2.6 presents the Laplace equation and can be rewritten with use of Laplacian operator ∇^2. For the rectangular coordinates 2.6 becomes

$$\frac{\vartheta^2 T}{\vartheta x^2} + \frac{\vartheta^2 T}{\vartheta y^2} + \frac{\vartheta^2 T}{\vartheta z^2} = \nabla^2 T = 0 \tag{2.7}$$

2.2 Convection

In the Convection mode, heat is transferred within a temperature gradient that exists between the surface of a body and the surrounding medium. The heat transfer consists of two mechanisms operating simultaneously: heat conduction and mechanical fluid transport. The fluid motion is a result of virtue of an external force. Depending on the nature of the external force , convection can be classified as forced , caused by a fan or a pump , or natural due to density gradient. The rate of heat transfer by convection between a surface and a fluid is determined by *Newton's Law of Cooling* [6]

$$q_c = \overline{h}_c A \Delta T \tag{2.8}$$

where ΔT is a difference between the surface temperature T_s and the temperature of the fluid T_∞ , $\overline{h}_c$ is an average heat transfer coefficient over area A. The value of $\overline{h}_c$ varies from 6 $W/(m^2 \cdot K)$ for natural air convection to 120000 $W/(m^2 \cdot K)$ for condensing of steam [9].
A quantitative evaluation of the convection heat transfer coefficient is a complex problem , as $\overline{h}_c$ is dependent on many variables such as geometry of the surface , flow characteristics , velocity and physical properties of a fluid, and temperature difference ΔT. The value of the heat transfer coefficient can also vary along the cooling or heating surface . However, for most engineering applications the average value $\overline{h}_c$ is often used instead.

2.2.1 Boundary-Layer Fundamentals

Consider a case of a fluid flowing past a plane surface. The flow region near the plate where the velocity of the fluid U_∞ is influenced by viscous forces is called the boundary layer. The distance from the plate at which the fluid velocity

achieves 99% of the free-stream velocity is called the boundary-layer thickness [6]. The velocity distribution along the plate surface is shown in the Fig. 2.3 Initially, the velocity profile is approximately parabolic and no mixing between layers at various distances from the plate occurs. The flow in this regime is called laminar flow. At some critical distance from the leading edge, mixing of the different layers due to developed eddies appears and transition from laminar to turbulent flow takes place.As it can be observed from the Fig. 2.3,there is a thin laminar sublayer near the plate surface , across which the velocity profile is nearly linear. Outside this sublayer the velocity profile becomes flat in the comparison to the initially developed laminar profile. The value of the Reynolds number, which will be presented in Subsection 2.2.5 is used to determine whether a flow is laminar or turbulent. For a plate, the transition takes place at $R_e = 5 \cdot 10^5$.

The boundary layer will also be developed in a tube flow. In this case , after a certain distance from the entrance , known as the starting length, the annular boundary layer of a tube grows together and forms fully developed flow. Depending on the Reynolds number, the fully developed flow can be either laminar or turbulent. Fig 2.4 shows the velocity distribution in a laminar (a) and a turbulent (b) flow inside the tube. For the fully developed laminar flow the velocity profile is parabolic, while for a turbulent flow it is again flatter as a result of radial mixing. For engineering calculations in a tube flow it is agreed that the transition takes place at $R_e = 2300$. When the wall is heated or cooled a thermal boundary layer, which is qualitatively similar to the velocity boundary layer is developed.

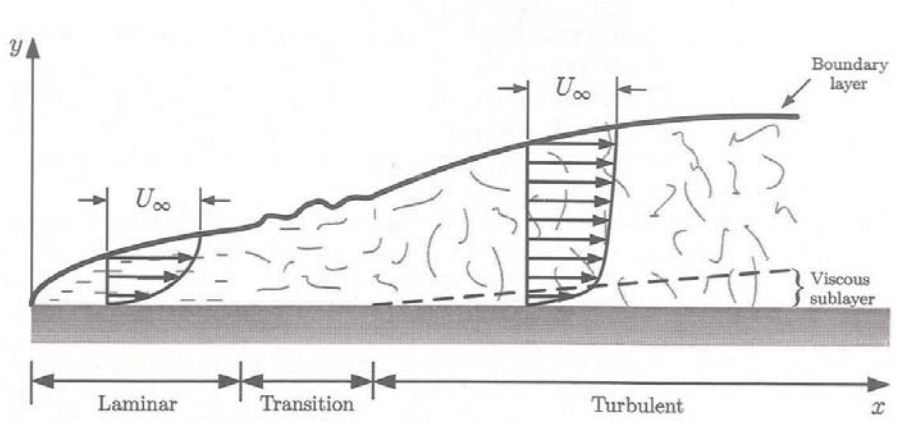

Figure 2.3: Velocity profile in a flow over a flat plate.

2.2.2 Incompressible Fluid Flow

The model of an incompressible fluid is based on the assumption that the fluid density is not affected by changes in the pressure [10]. The Navier-Stokes equations are the fundamental equations that describe the flow of the incompressible fluids. The Navier-Stokes equations for the three-dimensional volume of an

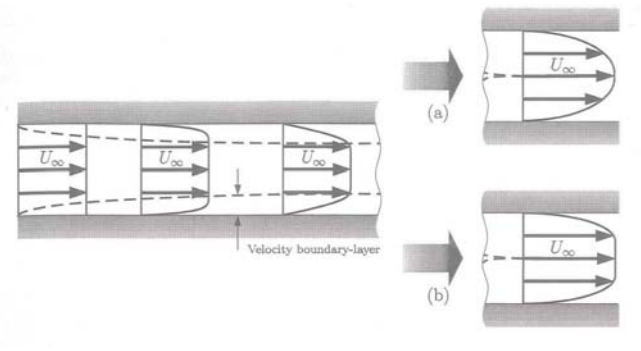

Figure 2.4: Velocity profile in a laminar (a) and a turbulent flow (b) inside a tube.

incompressible fluid in rectangular coordinates are presented by the following system of partial differential equation [11].

$$\begin{aligned}
\frac{\vartheta u}{\vartheta t} + u\frac{\vartheta u}{\vartheta x} + \upsilon\frac{\vartheta u}{\vartheta y} + \omega\frac{\vartheta u}{\vartheta z} &= -\frac{1}{\rho}\frac{\vartheta p}{\vartheta x} + \nu(\frac{\vartheta^2 u}{\vartheta x^2} + \frac{\vartheta^2 u}{\vartheta y^2} + \frac{\vartheta^2 u}{\vartheta z^2}) \\
\frac{\vartheta \upsilon}{\vartheta t} + u\frac{\vartheta \upsilon}{\vartheta x} + \upsilon\frac{\vartheta \upsilon}{\vartheta y} + \omega\frac{\vartheta \upsilon}{\vartheta z} &= -\frac{1}{\rho}\frac{\vartheta p}{\vartheta y} + \nu(\frac{\vartheta^2 \upsilon}{\vartheta x^2} + \frac{\vartheta^2 \upsilon}{\vartheta y^2} + \frac{\vartheta^2 \upsilon}{\vartheta z^2}) \\
\frac{\vartheta \omega}{\vartheta t} + u\frac{\vartheta \omega}{\vartheta x} + \upsilon\frac{\vartheta \omega}{\vartheta y} + \omega\frac{\vartheta \omega}{\vartheta z} &= -\frac{1}{\rho}\frac{\vartheta p}{\vartheta z} + \nu(\frac{\vartheta^2 \omega}{\vartheta x^2} + \frac{\vartheta^2 \omega}{\vartheta y^2} + \frac{\vartheta^2 \omega}{\vartheta z^2}) \\
\frac{\vartheta u}{\vartheta x} + \frac{\vartheta \upsilon}{\vartheta y} + \frac{\vartheta \omega}{\vartheta z} &= 0
\end{aligned} \tag{2.9}$$

where u ,υ,ω are the fluid velocities in the x,y,z directions,respectively, $\nu = \mu/\rho$ is the kinematic viscosity, μ is the absolute viscosity,and p is the pressure. The first three equations in the system 2.9 represent the equations of the motion (conversation of momentum) in three district dimensions and the fourth equation is the continuity equation (conversation of mass).
The system of Equations 2.9 in vector notation is given by [12]

$$\begin{aligned}
\frac{\vartheta \mathbf{u}}{\vartheta t} + \mathbf{u}\cdot\nabla\mathbf{u} &= -\frac{1}{\rho}\nabla p + \nu\nabla^2\mathbf{u} \\
\nabla\cdot\mathbf{u} &= 0
\end{aligned} \tag{2.10}$$

where $\mathbf{u} = (u, \upsilon, \omega)$. The symbol ∇ denotes the vector differential operator.

2.2.3 Energy Conservation Equation for a Laminar Flow

The principle of conversation of energy is applied to obtain the heat equation that couples the velocity field $\mathbf{u}$ and the temperature T. In compact vector notation the energy conservation equation is given by [6]

$$\rho c_p\frac{\vartheta T}{\vartheta t} + \nabla\cdot(-k\nabla T + \rho c_p T\mathbf{u}) = q_c \tag{2.11}$$

where c_p is the thermal capacity of the fluid at constant pressure. The expression within the brackets is the heat flux vector and q_c represents a heat source term.

2.2.4 Evaluation of Convection Heat Transfer Coefficients

According to [6], five general methods are available for the evaluation of heat transfer coefficients:

1. Dimensional analysis combined with experiments is a mathematically simple method and it is widely used for evaluation of heat transfer coefficients. However, the results obtained are rather coarse and cannot be treated without experimental verification. This method is described in detail in Subsection 2.2.5.

2. Exact mathematical solutions of the boundary-layer equations is a mathematically complex method, which requires simultaneous solution of the equations describing the fluid motion and transfer of heat in the moving fluid. The physical mechanism of the problem should be well understood to be described mathematically.

3. Approximate analysis of the boundary-layer equations by integral methods is a relatively simple method, which avoids the exact mathematical description of the fluid flow. Instead, the equation of motion and energy equation are applied to evaluate the heat transfer coefficients.

4. The analogy between heat and momentum transfer is a method used to analyze turbulent fluid flow. The K-ϵ model is one of the most frequently used turbulence models for engineering applications. Two additional transport equations are solved to obtain the turbulence kinetic energy K and the dissipation rate of turbulence energy ϵ [13]

5. Numerical analysis is a method used to solve, in an approximate form, the exact equations of motion. One of the most important advantages of this model is that once the solution procedure has been built , solutions for different boundary conditions, property variables, etc. can easily be computed.

2.2.5 Dimensional analysis

Dimensional analysis combines several variables to form a number of dimensionless groups. The main disadvantage of the method is that the results obtained from the calculations are incomplete and quite useless without experimental verification. Moreover the number of variables,influencing the physical process of heat transfer, should be properly selected beforehand. However , once the pertinent variables are known , dimensional analysis can be applied to most problems.

The Buckingham π theorem is used to determine dimensionless groups [6]. the five most important dimensionless groups are outlined below.

Reynolds number

The *Reynolds number* is a dimensionless ratio of inertia to viscous forces defined as

$$R_e = \frac{U_\infty L}{\nu} \tag{2.12}$$

where U_∞ is the velocity of the fluid, L is a characteristic length (which for a tube is the diameter) , and]nu is the kinetic viscosity. The size of the Reynolds number characterizes the flow of the fluid, i.e a low Reynolds number corresponds to laminar flow, while a high Reynolds number indicates turbulent flow.

Nusselt number

The *Nusselt number* is a dimensionless ratio of convection heat transfer to conduction in a fluid layer of thickness L. The Nusselt Number is defined as

$$N_u = \frac{\overline{h}_c L}{k_f} \tag{2.13}$$

where $\overline{h}_c$ is the average convection heat transfer coefficient and k_f is the thermal conductivity of the fluid.
With known Nusselt number, the heat transfer coefficient can easily be calculated from the definition given by Eq. 2.13.

Prandtl number

The *Prandtl number* is a dimensionless ration of the viscous boundary layer thickness to the thermal boundary layer thickness. The Prandtl Number is defined as

$$P_r = \frac{\nu}{\alpha} = \frac{c_p \mu}{k_f} \tag{2.14}$$

where c_p is the thermal capacity of the fluid at constant pressure and μ is the dynamic viscosity of the fluid.

Grashof number

The *Grashof number* is a dimensionless ration of buoyancy to viscous forces.The Grashof Number is defined as

$$G_r = \frac{g\beta(T_s - T_\infty)L^3}{\nu^3} \tag{2.15}$$

where g is acceleration due to gravity, and β is the volumetric thermal expansion coefficient. The Grashof Number characterizes the flow in natural convection and indicates whether it is laminar or turbulent.

Graetz number

The *Graetz number* is a dimensionless ratio defined as

$$G_z = \frac{\pi}{4} R_e P_r \frac{L}{l} \tag{2.16}$$

where l is the distance from the entrance of the channel. The Graetz number is used to define heat transfer coefficients in laminar tube flow.

2.3 Radiation

Thermal Radiation is a mode of heat transfer by which heat is transferred by electromagnetic waves from a body by virtue of its temperature. The heat transferred into or out of an object by thermal radiation is a function of several components, such as surface reflectivity, emissivity, surface area, temperature, and geometric orientation with respect to other participating objects. The heat rate emitted by the body to the surrounding is given by the *Stefan-Boltzmann's Law of thermal radiation* [6].

$$q_r = \sigma \epsilon A (T_s^4 - T_\infty^4) \tag{2.17}$$

where $\sigma = 5.67 \cdot 10^{-8} W/m^2 K^4$ is the Stefan-Boltzmann constant, ϵ is the emissivity of the body and A is the heat transfer area.

2.4 Thermal Resistance

Conduction describes heat transfer in any material through molecular collisions, lattice vibrations and unbound electron flow. The heat transfer rate in a material is given by Fourier's Law as described in Section 2.1.

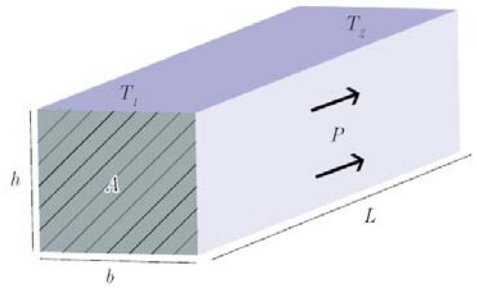

Figure 2.5: Heat transfer in one dimension, $T_1 > T_2$

From Figure 2.5 it can be seen that

$$dT/dx = \frac{T_2 - T_1}{L} \tag{2.18}$$

which gives

$$q_k = -\kappa A \frac{T_2 - T_1}{L} = \kappa A \frac{T_1 - T_2}{L} \tag{2.19}$$

By comparing Equation (2.19) to Ohms law for electrical circuits

$$q_k = \frac{\kappa A}{L} \cdot (T_1 - T_2) \equiv I = \frac{A}{\rho L} \cdot (U_1 - U_2) \tag{2.20}$$

the thermal and electrical analogy can be seen, giving the expression for thermal resistance as

$$R_{th} = \frac{L}{\kappa a} \tag{2.21}$$

In the cylindrical case it is assumed for simplicity that there is only heat transfer in the radial direction and the thermal resistance is derived in [14] for Figure 2.6 as

$$R_{th} = \frac{ln(r_o/r_i)}{\kappa L \varphi} \tag{2.22}$$

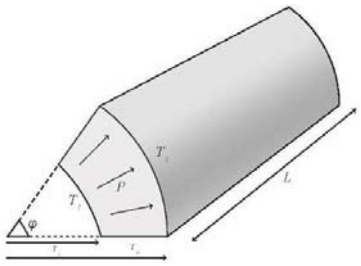

Figure 2.6: Heat transfer in the radial direction for a cylinder, $T_1 > T_2$

where $\varphi(rad)$ is the angle of the sector, r_o(m) and r_i (m) are the outer and inner radius of the cylinder.

Chapter 3

Theoretical Background

In this chapter a brief introduction to the theoretical background is given in order to fully understand the objective of this project. Different topics are treated, such as Silicon carbide (SiC) converters, switching losses, overview of measurements, calorimetry theory and error propagation.

3.1 Overview of SiC Semiconductors

During recent years, SiC power electronics has gone from being a promising future technology to being a potent alternative to state-of-the-art silicon (Si) technology in *high-efficiency* [4], *high-frequency*, and *high-temperature* applications. The reasons for this are that SiC power electronics may have lower voltage drops, higher voltage ratings, higher maximum temperatures, and higher thermal conductivities compared to the Si counterparts.

It is now a fact that several manufacturers are capable of developing high-quality transistors at cost that permit introduction of new products in application areas where the benefits of the SiC technology can provide significant system advantages. The additional cost for the SiC transistors in comparison with corresponding Si alternatives are significantly smaller today than the reduction in cost or increase in value seen from a systems perspective in many applications. Also, the dramatic quality improvement of the SiC material [15] in combination with excellent research and development efforts on the design and fabrication of SiC devices by several research groups has recently resulted in a strong commercialization of SiC switch-mode devices [15], [16]. However, the SiC device market is still in an early stage. The only available SiC switches are the bipolar junction transistor (BJT) [17], junction gate field-effect transistor (JFET) [16], [18], and metal-oxide-semiconductor field-effect transistor (MOSFET) [19], [20], which are still not in mass production. Special driver designs are required in order to use the advantageous performance of SiC devices compared to the Si counterparts. Such gate and base drivers should provide rapid switching for the SiC devices but the same time should also have the lowest possible power consumption. Furthermore, high-temperature operation is also preferable for these drivers because of the high-temperature capability of the SiC devices.

It is clearly shown that power electronics are moving into new areas because

of the features of SiC devices. When it comes to the design stage of power electronic converters with SiC devices instead of classic Si counterparts, three different design directions may be chosen (Figure 3.1). An itemized presentation of each single direction is given below:

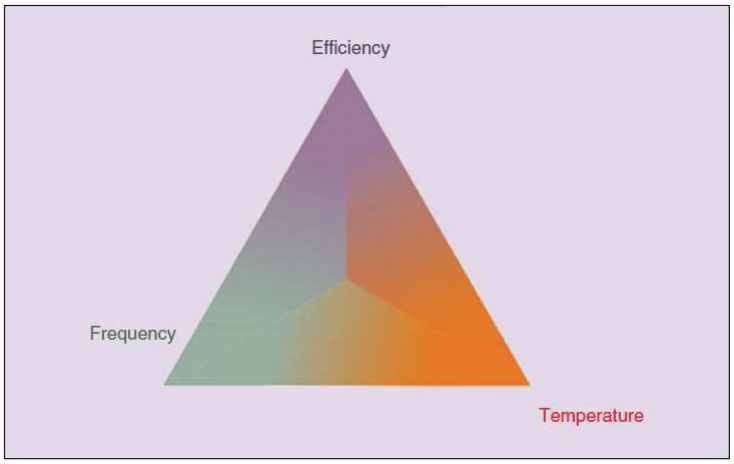

Figure 3.1: Different directions for SiC devices design [1]

- Since switching times in the range of nanoseconds have been reported, the most obvious direction is the increase of the switching frequency up to a few hundred kHz. In the case of the available Si devices for voltage ratings above 600 V, such high switching frequencies can only be reached when soft switching is employed [21]. From a system perspective, the design advantages are reduction of size and weight of passive elements (e.g., inductors, capacitors) [22]. This results in better compactness of the converter, especially in dc/dc converters and inverters with passive filters. Last but not least, the size of electromagnetic interference (EMI) filters will also be reduced [23], as the switching speeds are higher and the harmonics are shifted up to higher frequencies. Both short switching times and low voltage drops across SiC devices result in significant reduction of the power losses.

- In applications where the increase of switching frequency is not critical, one of the other two possible design directions might be chosen. A direct benefit is the reduction of size and weight of the cooling equipment [4], since an efficiency increase is equivalent to the reduction of the power losses.

- Furthermore, water cooling or air-forced cooling systems could be unnecessary as the amount of the dissipated heat is a few times lower compared to already existing devices (Si semiconductors). High efficiency is also important in power delivery and distribution systems as well as photovoltaic applications because the low power loss is directly recalculated into profit.

A new era in power electronics is entered [1] as new SiC transistors are introduced in high-efficiency, high-frequency, and high-temperature applications.

Efficiencies well above 99.5% [4] are possible in the power range of 10 –100 kW. High-quality samples of JFETs, BJTs, and MOSFETs are available, and within a few years, it is believed that mass-produced products using these new devices will be on the market in several application areas. The benefits of the new devices are so overwhelming that it cannot be afforded from the system perspective not to consider such devices.

Besides the strong points of these devices, power losses caused in SiC power devices should also be properly treated by the designer. The largest contribution of these losses is the sum of switching and conduction power losses.

3.1.1 Switching Losses

Several types of semiconductor power devices including BJTs, MOSFETs, GTOs, and IGBTs can be turned-on and off by control signals applied to the control terminal of the device. These devices are known as controllable switches and they are represented in a generic manner by the circuit symbol shown in Figure 3.2. When the switch is off, there is no current flown, while during on-state current can flow in the direction of the arrow only. The ideal controllable switch [24] has the following characteristics:

1. Block arbitrarily large forward and reverse voltages with zero current flow when off.
2. Conduct arbitrarily large currents with zero voltage drop when on.
3. Switch from on to off or vice versa instantaneously when triggered.
4. Vanishingly small power required from control source to trigger the switch.

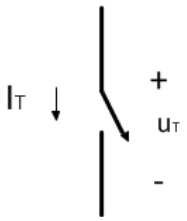

Figure 3.2: Generic controllable switch

Real devices, as we intuitively expect, do not have these ideal characteristics and hence they will dissipate power when they are employed in the numerous applications already mentioned. If the dissipated power is significantly high, the device might be thermally destroyed. Power dissipation in semiconductor power devices is fairly generic in nature; that is the same basic factors governing power dissipation apply to all devices in the same manner. The converter designer must understand what these factors are and how to minimize the power dissipation in the devices.

In order to estimate power dissipation in a semiconductor device, a controllable switch is connected in the simple circuit shown in Figure 3.3. This circuit models a very commonly encountered situation in power electronics. The current, which is flowing through a switch, it must also flow through some series

inductance. The dc current source approximates the current that would actually flow due to inductive energy storage. The diode is assumed to be ideal because the main focus is on the switch characteristics, though in practice the diode reverse-recovery current can significantly affect the stresses on the switch.

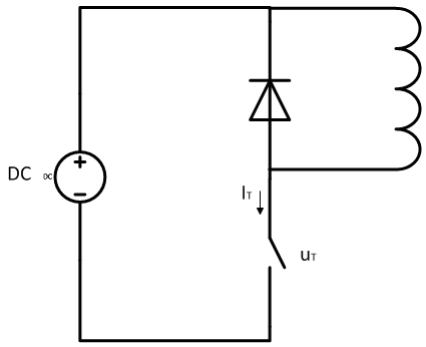

Figure 3.3: Generic-switch switching characteristics (linearized): simplified clamped-inductive-switching circuit

When the switch is on,the entire current I_o flows through the switch and the diode is reverse biased. When the switch is turned-off, I_o flows through the diode and a voltage equal to the input voltage V_d appears across the switch, assuming a zero voltage drop across the ideal diode. Figure 3.4b shows the waveforms for the current through the switch and the voltage across the switch, when it is operates at a switching frequency of $f_s = 1/T_s$, where T_s is the switching time period. The switching waveforms are represented by linear approximations to the actual waveforms in order to simplify the discussion.

When the switch has been turned-off for a while, it is turned on by applying positive control signal to the switch, as shown in Figure 3.4a. During the turn-on transition of this generic switch, the current buildup consists of a short delay time $t_d(on)$ followed by the current rise time t_{ri}. Only after the current I_o flows entirely through the switch voltage fall to a small on-state value of V_{on} with a voltage fall time of t_{fv}. The waveform in Figure 3.4b indicate that large values of switch voltage and current are present simultaneously during the turn-on crossover interval $t_c(on)$, where

$$t_{c(on)} = t_{ri} + t_{fv} \tag{3.1}$$

The energy dissipated in the device during this turn-on transition can be approximated from Figure 3.4b as

$$W_{c(on)} = \frac{V_d \cdot I_o \cdot t_{c(on)}}{2} \tag{3.2}$$

where it is recognized that no energy dissipation occurs during the turn-on delay interval $t_{d(on)}$.

Once the switch is fully on, the on-state voltage V_{on} will be in the order of $1\ V$ or so depending on the device, and it will be conducting a current I_o. The switch remains in conduction during the on interval t_{on}, which in general is much longer than the turn-on and turn-off transition times. The energy dissipation W_{on} in the switch during this on-state interval can be approximated as

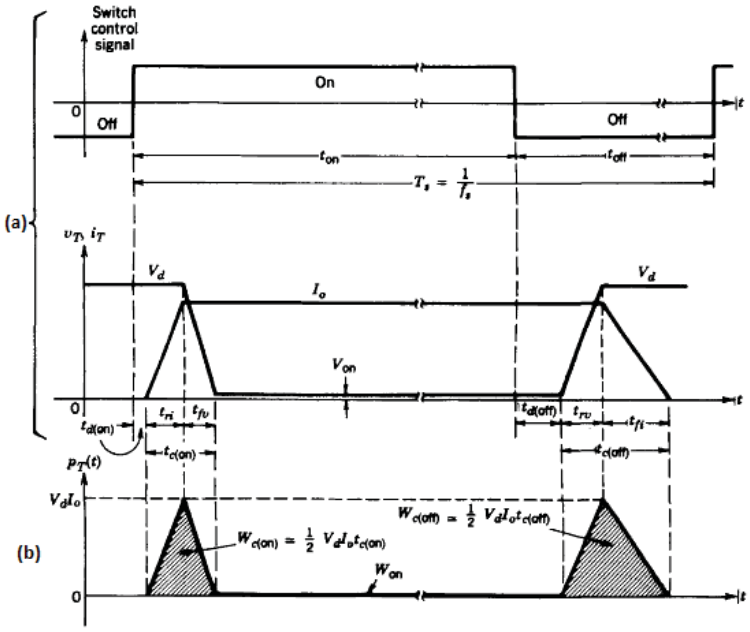

Figure 3.4: Generic-switch switching characteristics (linearized): (a) switch waveforms (b) instantaneous switch power loss

$$W_{on} = V_{on} \cdot I_o \cdot t_{on} \tag{3.3}$$

where $t_{on} >> t_{c(on)}, t_{c(off)}$

In order to turn the switch off, a negative control signal is applied to the control terminal of the switch. During the turn-off transition period of the generic switch, the voltage build-up consists of a turn-off delay time $t_{d(off)}$ and a voltage rise time t_{rv}. Once the voltage reaches its final value of V_d (see Figure 3.3) , the diode becomes forward-biased and starts conducting the current. The current in the switch falls to zero with a current fall time t_{fi} as the current I_o commutes from the switch to the diode. Large values of switch voltage and switch current occur simultaneously during the crossover interval $t_{c(off)}$ where

$$t_{c(off)} = t_{rv} + t_{fi} \tag{3.4}$$

The energy dissipated in the switch during this turn-off transition can be written, using Figure 3.4b

$$W_{c(off)} = \frac{V_d \cdot I_o \cdot t_{c(off)}}{2} \tag{3.5}$$

where any energy dissipation during the turn-off delay interval $t_{d(off)}$ is neglected since it is low compared to $W_{c(off)}$. The instantaneous power dissipation $p_T(t) = V_T i_T$ plotted in Figure 3.4b makes it clear that a large instantaneous power dissipation occurs in the switch during the turn-on and turn-off intervals. There are f_s such turn-on and turn-off transitions per second. Hence the

average switching power loss P_s in the switch due to these transitions can be approximated from equation 3.2 and 3.5.

$$P_s = \frac{1}{2} \cdot V_d \cdot I_o \cdot f_s \cdot (t_{c(on)} + t_{c(off)}) \tag{3.6}$$

This is an important result because it shows that the switching power loss in a semiconductor switch linearly varies with the switching frequency and the switching times. Therefore, if devices with short switching times are available, it is possible to operate them at high switching frequencies in order to reduce the filter requirements. The other major contribution to the power loss in the switch is the average power dissipated during the on-state P_{on}, which varies in proportion to the on-state voltage. From equation 3.3, P_{on} is given by

$$P_{on} = V_{on} \cdot I_o \cdot \frac{t_{on}}{T_s} \tag{3.7}$$

which shows that the on-state voltage in a switch should be as small as possible. The leakage current during the off state (switch open) of controllable switches is negligibly low, and therefore the power loss during the off state can be neglected in practice. Therefore, the total average power dissipation P_T in a switch equals the sum of P_s and P_{on}. From the considerations discussed above, the following characteristics in a controllable switch are desirable:

1. Low leakage current in the off state.
2. Low on-state voltage V_{on} to minimize the on-state losses.
3. Short turn-on and turn-off times. Thus, the device might be used at high switching frequencies.
4. High forward- and reverse-blocking-voltage capability. This will minimize the requirement for series connection of several devices, which complicates the control and protection of the switches. Moreover, most of the device types have a minimum on-state voltage regardless of their blocking voltage rating. A series of several such devices would lead to higher total on-state voltage drops and hence higher conduction losses. In most converter circuits, a diode is placed antiparallel to the controllable switch to allow reverse conduction of the current.
5. High on-state current rating. In high-current applications, this would minimize the need to connect several devices in parallel, thereby avoiding the problem of current sharing.
6. Low power consumption of the control unit. This might also simplify the control circuit design.
7. Capability to withstand the rated voltage and rated current simultaneously while switching. This will eliminate the need for external protection (snubber) circuits across the device.
8. Large dv/dt and di/dt ratings. This will minimize the need for external circuits otherwise needed to limit dv/dt and di/dt in the device so that it is not destroyed.

3.1.2 Conduction Losses

In addition to the switching losses, conduction losses are also an important component. A switching device when ON, behaves as an impedance which means that consumes energy. In general, the calculation formula of the conduction losses is presented in the following equation 3.8

$$P_{con} = I_{rms}^2 \cdot r_{on-D} \tag{3.8}$$

where I_{rms} is the rms value of the i_T and r_{on-D} is the on-state resistance of the switching device.

3.2 Typical ways of Power loss measurements

The previous mentioned methods do not provide an overall calculation of a converter losses as switching and conduction losses are a part of them. The aggregate amount also includes magnetic, bus bars and cable losses. Nowadays, there are standard ways of power loss measurement based on indirect power measurements or estimation methods. Indirect methods measure the inlet and outlet power of a device and calculate the power losses by subtracting them. However, the accuracy of such methods is usually low. On the other hand, estimation methods are based on electro-thermal power estimation which do not take into consideration several parameters and only depend on the environment conditions. Both method types are presented in this subsection.

3.2.1 Direct Watt-meter Measurement

In this method, the traditional electromechanical watt-meter is used to make measurements of the electrical power of the device or circuit under test. The watt-meter accuracy quickly is decreasing while the measured frequency is increasing, mostly when voltage and current waveforms are non-sinusoidal and contain high-frequency harmonics. This kind of watt-meter usually has low bandwidth and poor frequency response. Consequently, it is only applicable to dc and low-frequency sinusoidal measurement and is inappropriate for high-frequency and non-sinusoidal conditions.

3.2.2 Digital Measurements

Digital instruments, particularly digital oscilloscopes, are some of the most widely used measuring tools in power electronics systems today. The digital estimation of losses is based on the high-frequency sampling of voltage and current. For periodical power signals with voltage u(t) and current i(t), having a period of T, the average power P_0 is expressed as

$$P_o = \frac{1}{T} \int_0^T u(t) \cdot i(t) dt \tag{3.9}$$

The voltage and the current waveforms are simultaneously sampled at a sampling rate $f_{sampling} = 1/T_{sampling}$ and are converted to digital values. The the product of the digital values is the instantaneous power. If $v(t_i)$ and $i(t_i)$

are the instantaneous samples of the voltage and current at time $t_i = (iT/N)$, then the average power P_0 can be approximated by

$$P_d = \frac{1}{N} \sum_{n=0}^{N-1} u(t_i) i(t_i) \tag{3.10}$$

where N is the number of samples used for computing the average.

This method contains high inaccuracy due to the reading errors of the phase difference between voltage and current. In Figure 3.5 a function of the reading error versus the phase angle is clearly shown for several sample rate [2].

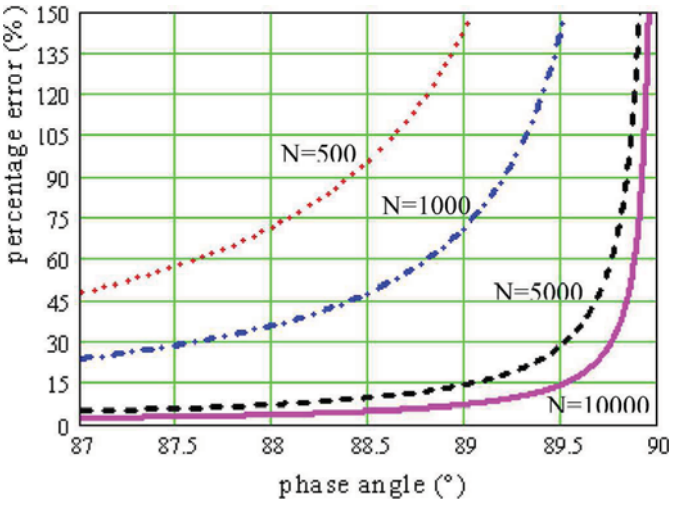

Figure 3.5: Inaccuracy percentage due to angle reading error for several samples [2]

In general, instrument reading errors refer to reading values. As the efficiency increases the power losses decrease. The problem is that even though the reading error is really low related to the total quantity, this error is multiple to the loss quantity. This is clearly stated in Figure 3.6. It is shown that when the converter efficiency is increasing the loss quantity uncertainty is exceeding 100% .

3.2.3 Electro-Thermal Estimation Method for SiC Converters

A measurement method based on electro-thermal properties of the converter is presented. This method is originally applied in a 40 kVA SiC inverter [4], built with Silicon Carbide Junction Field Effect Transistors (SiC JFET). A very low conduction loss has been achieved by parallel connecting ten 85 $m\Omega$ normally-on JFETs on each switching position.The main target is to reach efficiency higher than 99.5%, expecting low losses and free convection cooling. The philosophy of the method applied in the 40 kVA inverter is presented in this subsection. The basic assumption of the developed method is that the semiconductor power losses, regardless the type, either switching or conduction losses, cause the same

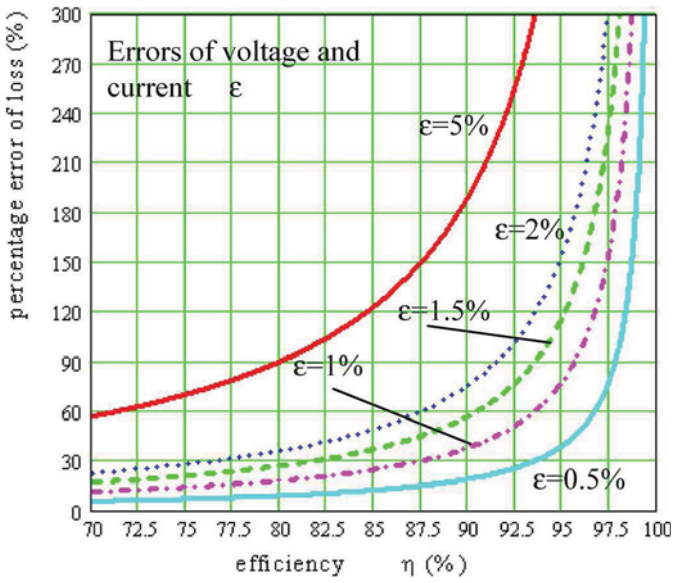

Figure 3.6: Power loss inaccuracy percentage as a function of voltage and current reading error [2]

temperature rise of the heatsink. The junction temperature, or just the heatsink temperature, could be used as a non-electrical measurable quantity. This quantity is representing the size of the power losses. Provided that a known reference case with a unique, precise, and reproducible relation between losses and temperature rise exists, the power losses occurring during inverter operation could be determined by comparison of the temperature rise in the reference case. Apparently, the characteristics of the average temperature T_{HAV} as a function of heating power must be defined first. For maximum accuracy, the reference case was achieved by feeding direct current through all JFETs (see Figure 3.7) and measuring the temperature of the heat sink (see Figure 3.8), the direct current, and the voltage drop across the JFETs.

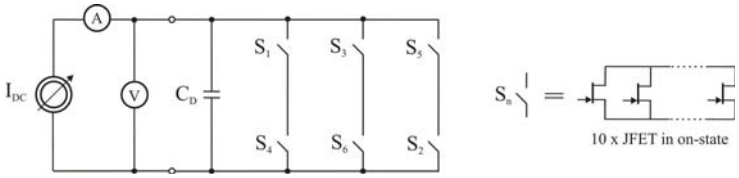

Figure 3.7: 40 kVA SiC inverter electrical-circuit schematic

In this way very accurate power measurements could be guaranteed at the same time as the loss distribution over the surface of the heat sink was the same as during normal operation. The total on-state resistance seen from the dc input is less than 10 $m\Omega$. Thus, a high-current and low-voltage regulated supply was required to reach ohmic power losses in the range of 150 W. Note, that the average temperature of the heatsink T_{HAV} in steady-state is easily observed as the back of the inverter is open. The 40 kVA SiC inverter model

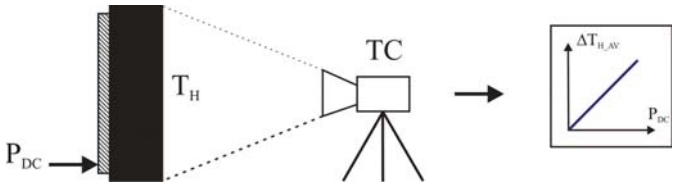

Figure 3.8: Measurement method of the experimental setup for dc current characterization

Number of Test	**Current Conditions**	**Power [W]**	**Temperature rise** $\Delta T[^oC]$
1	$I_{dc} = 80A$	38.5	12
2	$I_{dc} = 120A$	85.9	25.6
3	Variable current	100	28.3
4	Variable current	120	34.1

Table 3.1: DC current test results for the 40kVA

was characterized at various direct currents and power values where a typical heat-up test took approximately $1.5h$. Thermal camera images were recorded (see example in Figure 3.9) and analyzed every 5 minutes in order to ensure that steady-state conditions were established in each measurement case. Selected measurement data are collected and shown in Table 3.1. Because both the on-state resistance and the conduction losses change with temperature, tests with constant power have also been performed. The majority of the losses in the inverter are caused by conduction and strongly depends on temperature. Other part of losses caused by switching is almost temperature independent. That is why, neither constant direct current nor constant dc power test could provide exactly the same conditions of heating-up process as occur during the inverter operation. On the other hand, the main goal of characterization was to find reasonable T_{HAV} versus P_{DC} characteristics in steady-state, not to reproduce conditions of the inverter operation.

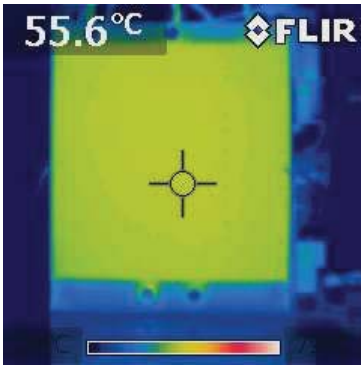

Figure 3.9: Thermal camera image of the inverter's heatsink during the dc current characterization

3.3 Calorimeter Theory

In theory, higher accuracy is achieved when power losses are measured directly. This is the main advantage of Calorimetry, power losses are measured as heat and associated error are also included in this quantity. In this way errors of up to 5% [3] are applied in the measured quantity and errors of indirect methods (Subsection 3.2) are avoided. Another great advantage is the ability to measure power losses(heat) regardless the type of the device under test (DUT). The fact that the calorimeter is limited at steady state is a disadvantage. Typical application areas to measure power losses are in magnetic components, capacitors, switching devices, power electronics and electrical machines.

3.3.1 Principles of Calorimetric Theory

Calorimetry is the technique of measuring the amount of heat dissipated during the thermal variations and especially for specific heat capacity measurement. Calorimetry considers the heat as a natural monetary quantity which uses calories and its derivatives as unit of measurement. Such units are defined as the temperature variation of different kind of materials and especially water when it is heated or cooled.
The heat measurement and in general calorimetry is based on two principles:

1. **Principle of the inverse changes:** The amount of heat produced or absorbed during a temperature variation is proportional to the mass of the material and proportional to the temperature difference.

2. **Principle of equality of heat exchange** The amount of heat absorbed during the temperature increase is equal to the amount of heat dissipated in the same material when this material is cooled, for the same temperature degrees.

3.3.2 Calorimetric techniques for Power loss measurements

Calorimetry is able to measure power losses directly, as heat, which dissipates from the DUT inside the chamber. This heat results in temperature rise from which total power losses can be determined. This heat in steady-state can be calculated through air flux and temperature measurement as indicated from equation 3.11.

$$P_{loss} = \dot{m} c_p \left(T_2 - T_1\right) \tag{3.11}$$

where T_1 and T_2 are the inlet and outlet temperatures, respectively, whereas c_p is the specific heat capacity of the fluid (air, water etc.).

Mass $\dot{m}$ is calculated as shown below:

$$\dot{m} = \dot{V} \rho \left(T_1\right). \tag{3.12}$$

where ρ is the fluid density at a specific temperature and $\dot{V}$ is the volume flow per time.

There are two types of calorimetric setups [25],open and close ones. A typical schematic of them is shown in Figure 3.10. In the open type calorimeter setup heat exchange is achieved by the direct contact of the DUT and the fluid (air). In

this case heat transfer is achieved by convection as described in Section 2.2. On the other hand, in the close type calorimeter the fluid is getting in touch with the DUT indirectly. The fluid is circulating in a closed loop circuit through which heat is transferred at temperature sensors. Simultaneously the flow of the fluid is measured by flux sensors. The heat is dissipating from DUT and through conduction the air temperature is increasing. Then heat is transferred in the same way from air to the pipes and then in the fluid. Assuming that the whole system is fully isolated from the environment the power losses are calculated based on energy increment, which is proportional to mass, specific heat capacity and temperature rise within a time frame. However, in real world the mass is not isolated enough which means that heat might leaks. In order to prevent final measurement inaccuracies the system has to be calibrated in order to recover the reliability of the measurement.

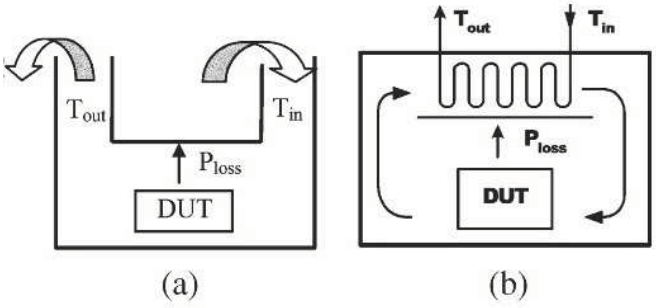

Figure 3.10: (a) Open (b) Closed Type Calorimeter

3.4 Error Propagation Theory

Science and engineering often involves measurements of different types. In engineering, geometrical quantities (such as angles, distances, heights) , physical quantities (gravity) or electrical quantities (voltage, current) are measured, producing large quantities of data which need to be treated. Human limitations, imperfect instruments, unfavorable physical environment and unsuitable measurement procedures define the measurement condition. Influenced by the measurement conditions, all measurement results contain errors. Measurement errors can be discovered in different ways. If the same measurement is repeated several times, different results will be obtained due to measurement errors. Also, a more accurate way to discover errors is to check whether the obtained measurement results satisfy physical relations, which may exist.

Normally, one may distinguish three types of errors [26] : *systematic errors*, *gross errors* and *random errors*.

- *Systematic errors* are errors which follow certain mathematical or physical rules and often affect surveying results systematically. The reasons for this kind of errors can be the instruments as such, physical environment in which measurements are made or even human factors and measurement

procedures. To avoid or reduce systematic errors, calibration of the instruments is needed. Furthermore, design and use of suitable measurement procedures can reduce or eliminate possible systematic errors and last but ot least is the correction of measurement results afterwords. One example of systematic errors is the constant error of 10 V for voltage measurement instrument. This constant error will cause a systematic error to all voltage measurements by this instrument.

- *Gross errors* are errors due to human mistakes, malfunctioning instruments or wrong measurement methods. Gross errors cannot be treated by statistical methods because they do not follow certain rules. In principle, gross errors are not permitted and should be avoided by human carefulness and control routines. For example, it can happen when data are not transferred in an appropriate way at a paper and a digit is wrong(5.21 instead of 5.1).

- *Random errors* or stochastic errors are errors which behave randomly and affect the measurements in a non-systematic way. The sources of random errors can be be human factors, instrument errors, physical environment and measurement procedures. They can be reduced by improving the total measurement condition. The primary study object of theory of errors is explicitly random errors. Probability theory and mathematical statistics is the science which is specialized and focused in studying random events, variables and functions. It constitute the theoretical background for random measurement errors treatment.

Assuming a quantity z which is a function of measured quantities x and y, $z = h(x, y)$. By expanding h as a Taylor series around the mean value of the input variables result to equation 3.13:

$$h(X,Y) = h(\mu_x, \mu_y) + \left(\frac{\vartheta h}{\vartheta x}\right)(X - \mu_X) + \left(\frac{\vartheta h}{\vartheta y}\right)(Y - \mu_Y) + h.o.t. \qquad (3.13)$$

where *h.o.t.* stands for *higher order terms*.

A Taylor expansion like this is only valid if the neglected higher-order terms, like, $\frac{1}{2}\left(\frac{\vartheta^2 h}{\vartheta x^2}\right)(X-\mu_X)^2$ are small compared to the included terms, like $\left(\frac{\vartheta h}{\vartheta x}\right)(X-\mu_X)$. So it is necessary that:

$$\begin{aligned} \left(\frac{\vartheta h}{\vartheta x}\right)(X - \mu_X) &>> \frac{1}{2}\left(\frac{\vartheta^2 h}{\vartheta x^2}\right)(X - \mu_X)^2 \\ \left(\frac{\vartheta h}{\vartheta x}\right) &>> \frac{1}{2}\left(\frac{\vartheta^2 h}{\vartheta x^2}\right)(X - \mu_X) \\ \frac{2\left(\frac{\vartheta h}{\vartheta x}\right)}{\left(\frac{\vartheta^2 h}{\vartheta x^2}\right)} &>> (X - \mu_X) \end{aligned} \qquad (3.14)$$

And similarly for Y. We can have this happen either if $(X\mu_X)$ is always very small, or if the ratio of the first to the second derivative is always very large that is, the function h is smooth.

- **Assumption 1: Measurement errors are small, where the scale for smallness is set by the ratio of first to second derivatives.**

If *Assumption 1* holds, and Taylor expansion can be used, h is expressed as a linear combination of random variables,where it is know how to handle linear combinations. First, the mean:

$$\begin{aligned}
E[Z] = E[h(X,Y)] &= h(\mu_X,\mu_Y) + E\left[\left(\frac{\vartheta h}{\vartheta x}\right)(X-\mu_X)\right] + E\left[\left(\frac{\vartheta h}{\vartheta y}\right)(Y-\mu_Y)\right] \\
&= h(\mu_X,\mu_Y) + \left(\frac{\vartheta h}{\vartheta x}\right)E\left[X-\mu_X\right] + \left(\frac{\vartheta h}{\vartheta y}\right)E\left[Y-\mu_Y\right] \\
&= h(\mu_X,\mu_Y) + \left(\frac{\vartheta h}{\vartheta x}\right)(E[X]-\mu_X) + \left(\frac{\vartheta h}{\vartheta y}\right)(E[Y]-\mu_Y) \\
&= h(\mu_X,\mu_Y) + \left(\frac{\vartheta h}{\vartheta x}\right)(\mu_X-\mu_X) + \left(\frac{\vartheta h}{\vartheta y}\right)(\mu_Y-\mu_Y) \\
&= h(\mu_X,\mu_Y)
\end{aligned}$$

Now the variance may be computed:

$$\begin{aligned}
Var(Z) = Var(h(X,Y)) &= Var(h(\mu_x,\mu_y) + \left(\frac{\vartheta h}{\vartheta x}\right)(X-\mu_X) + \left(\frac{\vartheta h}{\vartheta y}\right)(Y-\mu_Y)) \\
&= Var(\left(\frac{\vartheta h}{\vartheta x}\right)(X-\mu_X) + \left(\frac{\vartheta h}{\vartheta y}\right)(Y-\mu_Y))
\end{aligned}$$

The term $h(\mu_X,\mu_Y)$ can be dropped because it is constant. Now an additional assumption is needed.

- **Assumption 2: The measurement errors in the input variables are independent.**

$$\begin{aligned}
Var(Z) &= Var(\left(\frac{\vartheta h}{\vartheta x}\right)(X-\mu_X)) + Var(\left(\frac{\vartheta h}{\vartheta y}\right)(Y-\mu_Y)) \\
&= \left(\frac{\vartheta h}{\vartheta x}\right)^2 Var(X-\mu_X) + \left(\frac{\vartheta h}{\vartheta y}\right)^2 Var(Y-\mu_Y) \\
&= \left(\frac{\vartheta h}{\vartheta x}\right)^2 \sigma_X^2 + \left(\frac{\vartheta h}{\vartheta y}\right)^2 \sigma_Y^2
\end{aligned}$$

Taking the square root of Var(Z) to get the standard deviation gives us the usual formula for propagation of error.The most important special case for this is when the values of x and y we plug in to the formula are themselves obtained by averaging many measurements - that X, above, is really X, and Y is really Y. The following assumptions can be made:

- **Assumption 3: Measurement errors are independent from one measurement to the next.**

- **Assumption 4: There are many measurements of each variable.**

In this case, the central limit theorem may be used to say more about $\overline{X}$ and $\overline{Y}$. The mean values of $\overline{X}$ and $\overline{Y}$ are still the population means, μ_X and μ_Y. But now the standard deviations plugged in are standard errors, $s_x = \sigma_X/\sqrt{n}$ and $s_y = \sigma_Y/\sqrt{n}$. Also, $\overline{X}$ and $\overline{Y}$ are Gaussian. Since a linear combination of independent Gaussians is Gaussian, Z is also Gaussian. So the following results are obtained:

Suppose $Z = h(\overline{X}, \overline{Y})$, where $\overline{X}$ is the sample mean of measured values of X, and likewise for Y. Then, if Assumptions 1 to 4 hold, Z is approximately Gaussian, with mean $\mu_Z = h(\mu_X, \mu_Y)$, variance

$$\sigma_Z^2 = \left(\frac{\vartheta h}{\vartheta x}\right)^2 \frac{\sigma_X^2}{n} + \left(\frac{\vartheta h}{\vartheta y}\right)^2 \frac{\sigma_Y^2}{n} \tag{3.15}$$

and *Standard Error*

$$\sigma_Z = \sqrt{\left(\frac{\vartheta h}{\vartheta x}\right)^2 \frac{\sigma_X^2}{n} + \left(\frac{\vartheta h}{\vartheta y}\right)^2 \frac{\sigma_Y^2}{n}} \tag{3.16}$$

In this point, it is easy to prove that if $Z = h(\overline{X}, \overline{Y}, \overline{W})$,where $\overline{X}$ is the sample mean of measured values of X, and likewise for Y and W, and Assumptions 1 to 4 hold , Z is approximately Gaussian, with mean $\mu_Z = h(\mu_X, \mu_Y, \mu_W)$, and *Standard Error* :

$$\sigma_Z = \sqrt{\left(\frac{\vartheta h}{\vartheta x}\right)^2 \frac{\sigma_X^2}{n} + \left(\frac{\vartheta h}{\vartheta y}\right)^2 \frac{\sigma_Y^2}{n} + \left(\frac{\vartheta h}{\vartheta w}\right)^2 \frac{\sigma_W^2}{n}} \tag{3.17}$$

By knowing the mean value of Z (μ_Z) and the standard error (σ_Z) it is easily stated that the measurements of Z are in the space:

- $[\mu - \sigma, \mu + \sigma]$ with a probability of ***68.2%***
- $[\mu - 2\sigma, \mu + 2\sigma]$ with a probability of ***95.4%***
- $[\mu - 3\sigma, \mu + 3\sigma]$ with a probability of ***99.6%***

This distribution is clearly shown in Figure 3.11 where dark blue represents the $[\mu - \sigma, \mu + \sigma]$, between the lighter blue is the space for $[\mu - 2\sigma, \mu + 2\sigma]$ and the rest for $[\mu - 3\sigma, \mu + 3\sigma]$.

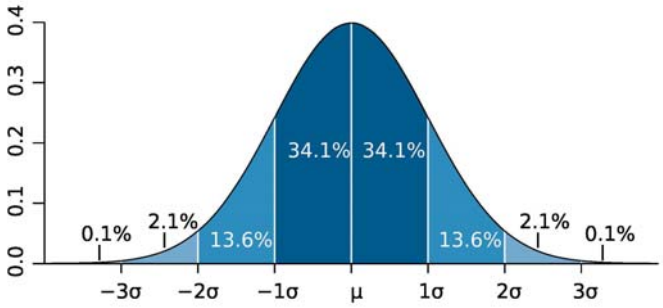

Figure 3.11: Normal distribution curve that illustrates standard deviations

Chapter 4

Design Process of the Calorimeter

In this chapter the design and construction processes are presented. Moreover a detailed report of the selection criteria, philosophy, dimensioning, equipment selection and implementation are also discussed.

4.1 Calorimetric Type Selection

After the theoretical background a more detailed approach is needed. The next step is the selection of which specific type of calorimeter type (open or closed) to implement. As the motivation of this work is high accuracy, it has to be one of the main selection criteria. In Figure 4.1 [3] there is an overview of different implemented calorimeters and their accuracies ([3], [27], [28], [29], [30], [31], [32], [33], [34], [35], [36], [37]). It is clearly stated that the closed type calorimeters in general are more accurate than the open type ones. However, open type setups exhibits a few advantages that make their construction and operation more efficient in comparison to others:

1. **Simple Design:** In comparison to a closed type setup it is more simple and efficient to design an open-type calorimeter. An open type setup consists of a simple chamber, one inlet and one outlet pipe, as shown in Figure 3.10. Most of the closed type setups use a double-jacketed chamber in order to achieve high accuracy which leads to a more complex construction.

2. **Overheating - Cooling:** As mentioned in [3] most of the closed type calorimeters require a measurement duration longer than two hours. Inside a closed chamber, the air does not circulate and renewed as the heatsink designer initially calculated. This time period without the appropriate cooling is able to stress or even destroy the DUT. In open type calorimeter both measurement process and cooling are performed in a way that there is no concern about overheating of the DUT and the performance whole process.

3. **Short Time Repeatable Measurements:** Because of the cooling ability of the system, the chamber is able to measure in a very short time after a previous measurement. This ability does not characterize closed type setups because extra equipment is required.

4. **Low Cost:** The necessary equipment needed for an open type implementation costs less than the sophisticated equipment required for closed type setups. Moreover, pipes and the rest of the components are originally made for ventilation purposes and are easily obtained.

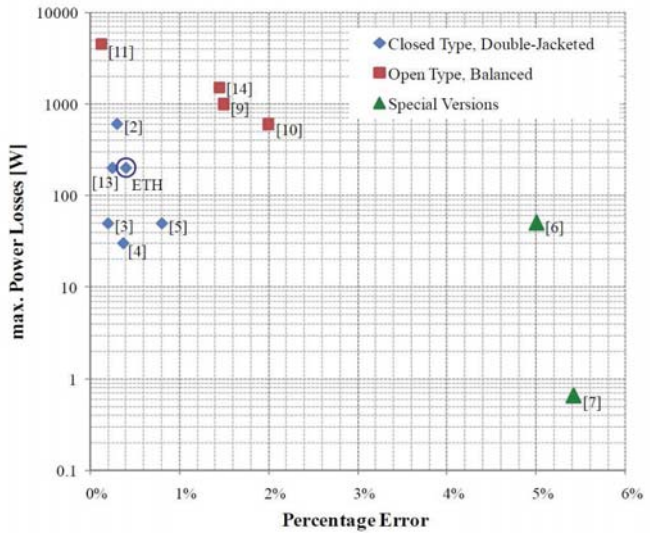

Figure 4.1: Overview of different implemented calorimeters and their accuracies. This figure was taken from [3]. The references of this figure correspond at the references of the source.

As a result of all mentioned above, the author of this thesis decided that an open type calorimetric setup is more appropriate to implement than any other type (closed , closed double-jacketed). Figure 4.2 present a simple schematic diagram of this setup.

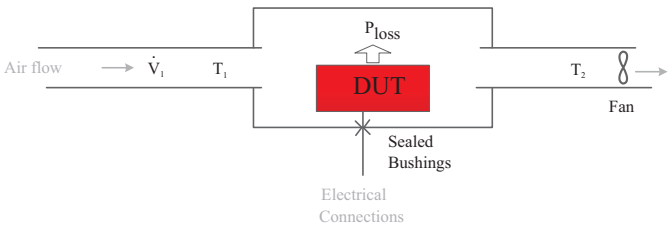

Figure 4.2: Schematic diagram of the calorimeter proposed in this thesis

4.2 Open Calorimeter Theory - Philosophy

As shown in Figure 4.2 there is a fan which forces air through the inlet pipe, chamber and outlet pipe respectively. This amount of air is heated by the DUT and as a result heat is transposed by means of air. The inlet and outlet temperature as well as the air flow are measured. Combining Equations 3.11 and 3.12 results in Equation 4.1, which is the calculation formula for power losses as shown below:

$$P_{loss} = \dot{V} \cdot \rho \cdot c_p \cdot (T_2 - T_1) \tag{4.1}$$

where $\dot{V}$ is the volume variation in m^3/s , ρ is the air density in kg/m^3 , c_p is the specific heat capacity in $J/(Kg \cdot K)$ and temperature T in ^oC (or K), whereas indication $_1$ refer to inlet air quantities and indication $_2$ to outlet air quantities.

4.3 Dimensioning - Constraints

In order to continue with the system implementation an analysis on the constraints and requirements should be done. Below, there is a list of the most important ones:

- The power loss to be measured is between 0 W to 300 W
- The inlet temperature is close to 20^oC (Ambient Temperature)
- The minimum temperature difference (ΔT) in order to achieve high accuracy
- The air flow bounds

To start with, the properties of air are shown in Table 4.1. What it is clearly shown is that the difference of heat capacity from 20^oC to 80^oC is negligible and lower than 0.2%. However, it is critical to avoid this error and take into account the heat capacity variation.

Air properties at a specific temperature which are not in Table 4.1 are obtained using *linear interpolation* between the closest temperatures. The calculation formulas are shown in the following Equations 4.2, 4.3 and the calculation algorithm is appended in appendix A

$$C_{p_{T_1}} = C_{p_{T_a}} + (C_{p_{T_b}} - C_{p_{T_a}}) \cdot \frac{(T_1 - T_a)}{(T_b - T_a)} \tag{4.2}$$

$$\rho_{T_1} = \rho_{T_a} + (\rho_{T_b} - \rho_{T_a}) \cdot \frac{(T_1 - T_a)}{(T_b - T_a)} \tag{4.3}$$

Figure 4.3 depicts a first approach of the design. Airflow over $0.03m^3/s$ results in a ΔT less than 5^oC which causes a critical overall error. It is necessary to set an upper air flow boundary at 0.03 m^3/s and a minimum ΔTat 5^oC in order to avoid high inaccuracy as shown in Figure 4.4

Temperature	**Density**	**Specific Heat Capacity**
T (^oC)	$\rho(kg/m^3)$	$c_p(kJ/kgK)$
-150	2.897	1.016
-100	2.046	1.008
-50	1.584	1.006
40	1.293	1.006
20	1.205	1.006
40	1.127	1.007
60	1.060	1.008
80	1.000	1.010
100	0.946	1.011
150	0.834	1.017
200	0.746	1.025
300	0.616	1.045
400	0.524	1.069
500	0.456	1.093
750	0.345	1.144
1000	0.277	1.193
1500	0.199	1.282
2000	0.155	1.468
2500	0.126	2.200

Table 4.1: Air Properties

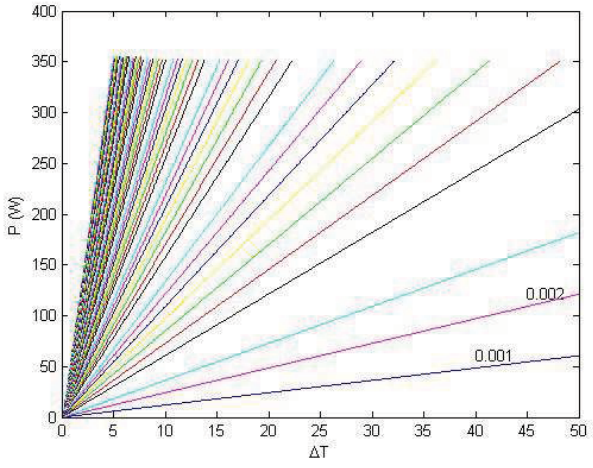

Figure 4.3: Power losses as a function of ΔT , for different air flow starting from 0.001 m^3/sec

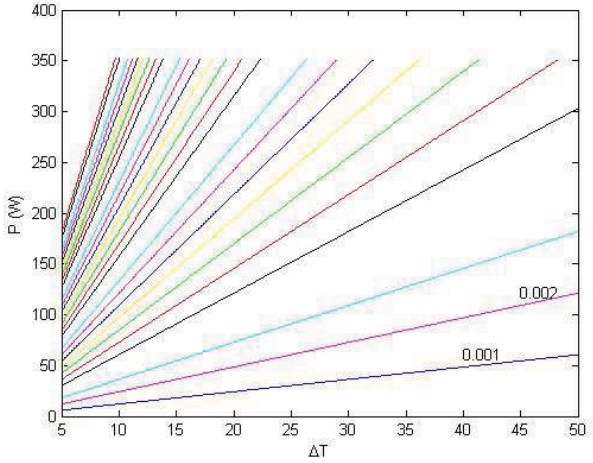

Figure 4.4: Power losses as a function of ΔT, limited to minimum $\Delta T = 5^oC$ and maximum air flow equal to $0.03m^3/s$

4.4 Sources of Inaccuracy and Possible Remedies

Beside the fact that the previously taken constraints were followed, errors may appear which come from various sources. Most of them are partially treated or even erased. In any case, the inaccuracy introduced will be a percentage of the overall error. Typical sources of errors error sources are the measurement instruments, the heater power used for calibration and leakage through the chamber walls.

4.4.1 Temperature measurement

In order to measure the inlet and outlet temperatures the system is equipped with two thermocouples. Various thermocouples are available in the market offering either high accuracy or fast measurements. Typical values for the accuracy of thermocouples are approximately $1 - 1.5^oC$ which offer a quick response to temperature variation. However, a better accuracy might be achieved at a cost of slower response time. Even if PT100 is too slow to accurately detect the temperature variations, it can achieve an error of $\pm 0.2^oC$. Nevertheless, the purpose of this thesis is to reach highly-accurate measurements in steady-state operation of the DUT. Thus, the time latency counts as a less important issue. It must be kept in mind that the temperature of the instrument, as such, is also rising due to the current circulating through it, as a measuring signal. This problem can be actually treated by supplying the same value of dc current to both the inlet and the outlet PT100 sensors. Assuming that this temperature offset affect both sensors and taking into consideration that it is only the temperature difference that is introduced in Equation 3.11, it is obvious that error is canceled.

4.4.2 Air flow measurement

Another critical quantity is the air flow. Most of the instruments are able to measure the total and static pressures and they produce a reading of the dynamic pressure. Then the air velocity and the air flow are calculated as shown in Equations 4.4 and 4.5, respectively:

$$AirVelocity : v_{air} = \sqrt{P_d} \tag{4.4}$$

$$Airflow : Q = S \cdot \sqrt{P_d} \tag{4.5}$$

where P_d is the dynamic pressure, whereas S is the duct section. The dynamic pressure is measured as a function of static and total pressure. In sensing static pressure a big effort has been made in order to eliminate the effect of air movement. In order to determine the dynamic (velocity) pressure, it is necessary to determine these effects fully and accurately. This is usually done with an tube which faces directly into the air stream. This type of sensor is frequently called a "total pressure pick-up" since it receives the effects of both static pressure and dynamic pressure. In Figure 4.5, separate static connections (a) and total pressure connections (b) can be connected simultaneously across a manometer (c). Since the static pressure is applied to both sides of the manometer, it is canceled out and the manometer indicates only the dynamic pressure.This kind of instruments have a significantly extended error of 3-5%, which is usually considered as unacceptable.

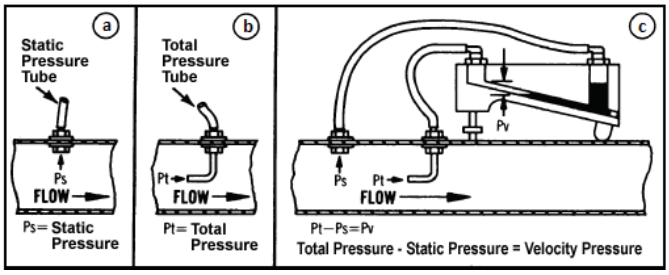

Figure 4.5: Manometer: (a) static (b) total (c) dynamic pressure measurement types

The method mentioned above is based on air force, in opposition to another group of air velocity instruments known as anemometers which directly measure the air velocity. Anemometers consists of a motor with a vane which rotates and produce the desired signal (rotational frequency). The reading error of this method is lower than 1% .

4.4.3 Leakage

As already mentioned above, one main source of error in the calorimetric measurement is the heat leakage through the test chamber walls. A proper isolation and a suitable design of the chamber are both required in order to minimize this effect. Consequently , materials with low heat capacity and extremely low thermal conductivity should be used in order to achieve a high enough thermal

resistance. Thermal resistance of the chamber and power losses through the wall are calculated using Equations 4.6 and 4.7, respectively:

$$R_{th} = \frac{d_{wall}}{\lambda A_{wall}} \tag{4.6}$$

$$P_{wall} = \frac{T_{Chamber} - T_{Ambient}}{R_{th,wall}} \tag{4.7}$$

Moreover, another source of error is the mass leakage through the various connections of the equipment. The fan, which is mounted in the outlet pipe, can transpose a constant amount of air. This air flows from the inlet pipe and the air leakage points, as for instance, the pipe-chamber connections and the chamber cover. If this leakage is not properly treated, the air flow instrument will measure the wrong amount of air transposed, resulting in an underestimation of the power produced in the DUT. This leakage can be easily avoided by properly isolate all the "weak" points of the chamber.

4.4.4 Heater power

A part of great importance is the heater power. It consists of several power resistors, spread in the chamber which cover the area of a typical converter. They are supplied by a dc current aiming to heat the chamber and acting as a DUT with a known power in order to calibrate and test the accuracy of the system. Possible errors might be introduced with the measurement of the dc voltage and current. Such errors can be easily reduced to very low values by using high-end multimeters. The heater power will be used in the calibration process which is described in Section 5.1

Discussion

As mentioned above, several of the inaccuracies can be eliminated by calibrating the calorimeter employing an ohmic heater. A basic requirement of this method is to ensure that the power of the heater can be determined with the highest possible accuracy. If the heater is fed with a dc current a very high accuracy can be reached, even using normal high-end multimeters. Thus, this measurement has no big impact on the overall error. With regard to the mass flow, calibration shifts the focus on the efforts at reducing the power error from measurement accuracy to repeatability. For example the exact flow rate is of low importance if the same flow conditions can be achieved during the DUT as during the the calibration process.

4.5 Equipment

It is now necessary to define the DUT and its physical dimensions. This practically means that the dimensions of the chamber must be such to fit the power electronics converters which are going to be evaluated. It should be kept in mind, that very high efficiencies can be achieved, for instance, by employing SiC power transistors. In this case, however, the compactness of the systems is also possible due the the smaller size and volume of the passive components

and the absence of large cooling equipment [38]. Therefore, the chamber was selected according to the DUT with inner dimensions of 355 mm x 265 mm x 545 mm and wall thickness of 48 mm. It is made by Expandable Polystyrene (EPS) with a thermal conductivity of 0.035 W/mK (Figure 4.6). The very low thermal conductivity is needed in order to achieve high thermal resistance and as a result to get rid of any heat leakage.

Figure 4.6: A 355mm x 265mm x 545mm chamber made by EPS used in this project

Two pipes are placed in the chamber as shown in Figure 4.6 with a diameter of 100 mm. They are also made by plastic for heat leakage reasons and low heat capacity.

For temperature measurement the selection process which was followed has been described in Section 4.4.1. Two PT100 sensors (RTI-400-DIN-200-B-8-0) are mounted in the inlet and outlet pipes, as illustrated in Figure 4.7, in order to measure the inlet and outlet air temperature, respectively. According to the manufacturer, the accuracy of the sensors is better than $\pm$ 0.2 ^oC in a range of -50 – 400 ^oC. The resistance of the PT100 sensors vary with respect to the temperature. Equation 4.8 gives the correlation between the measured resistance of the PT100 sensors and the temperature.

$$T_{PT100} = \frac{(R_{PT100} - 100)}{0.038} \tag{4.8}$$

Regarding the air flow, an ac fan is used with an air transpose capability of 0.051 m^3/sec. The fan (System-air K 100 M Circular duct fan) is supplied by a speed controller (SEN-EVS-0-X-DT). Depending on the desired air flow, the output voltage of the controller can vary between 0 – 230 V. Both of them are shown in Figure 4.8 and 4.10, respectively. The air flow measurement equipment (MiniAir64 shown if Figure 4.9) is able to measure air speeds up to 40 m/s with an accuracy of 1%. The output signal is a dc current between 4–20 mA as a linearized function of the reading.

In last step, a compact-RIO (NI cRIO-9074) was used in order to implement

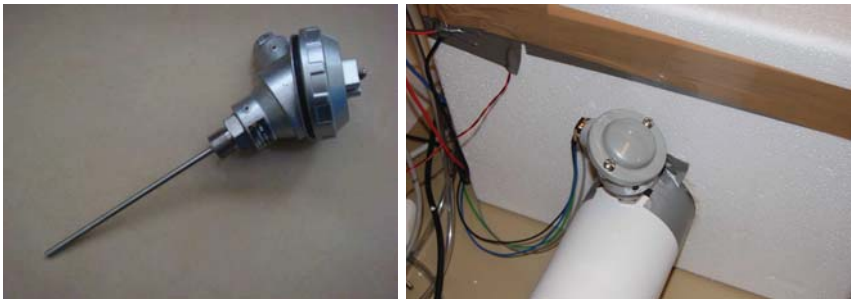

Figure 4.7: PT100 temperature measurement instruments mounted in the pipes.

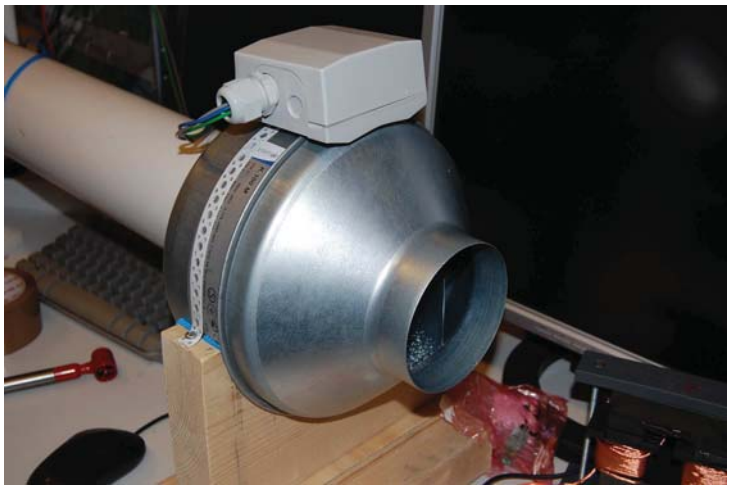

Figure 4.8: Induction motor originally made for ventilation purposes.

Figure 4.9: MiniAir64 mounted in the outlet pipe.

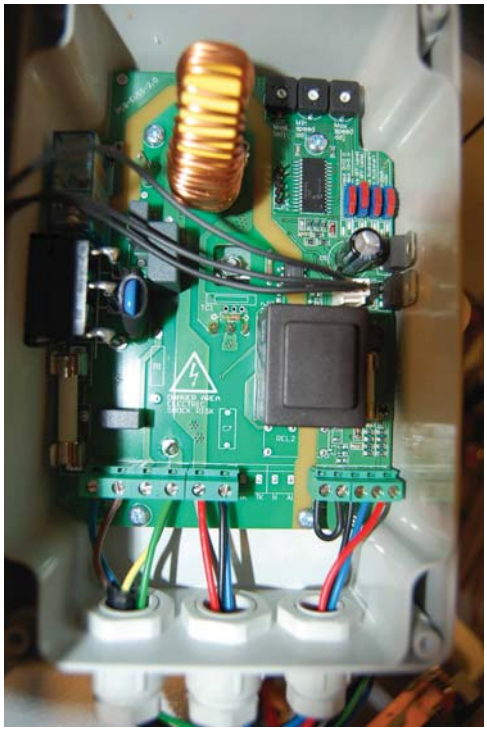

Figure 4.10: Speed controller for the control of the induction motor

the control and the measuring system. It consists of a processor running at 400 MHz and 128 MB of RAM. The real-time operations are handled by a Spartan–3 2M FPGA and several I/O and communication ports are included such as Ethernet and RS-232. The cRIO also communicates with a host computer where several processes are running and the graphic user interface (GUI) exists. Additionally, the cRIO is equipped with modules which serve as either input or output interfaces. One current output source (NI 9265) and one voltage input (NI 9219) modules are used to communicate and control the whole system. The cRIO and the NI modules are depicted in Figure 4.11.

A detailed list of the equipment used for the construction is shown in Table 4.2

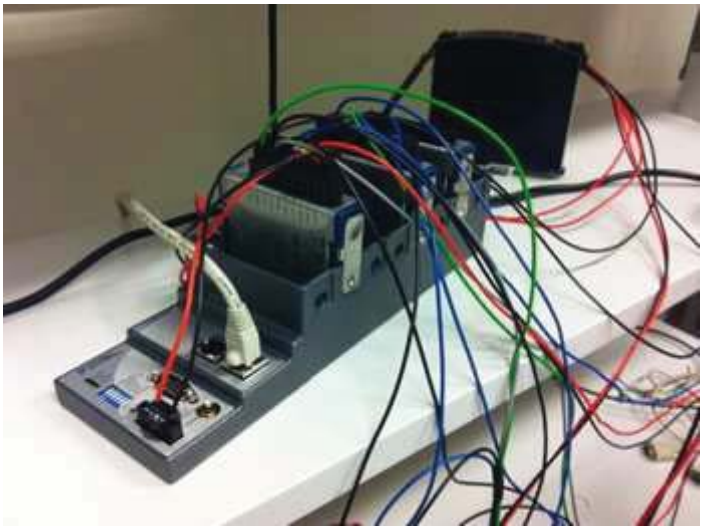

Figure 4.11: The compact-RIO connected with the sensors and the network

4.6 Implementation

Every part of this setup is now properly connected in the setup and in Compact-RIO. Input and output signals are handled by an algorithm which gather every information.

4.6.1 Measurement and Control Algorithm

Every instrument feeds the cRIO with its measurement value as either a voltage or current signal. The input signal module reads this signal and converts it from analog to digital. The FPGA module handles the measurement reading process which operates faster in comparison to the processes running in the host computer. Then, the values are transfered from the FPGA to the host computer. Everything is scaled at its dimensions according to the instrument's constructor. An outline of FPGA-host computer communication is shown in Figure 4.12. Later, the main algorithm is running and calculating the final values of the measurement according to the block diagram shown in Appendix

Sensor	**Type**	**Parameters**
Temperature	$PT100$	Measuring Range: -50^oC – $+400^oC$ Accuracy: $\pm 0.2^oC$
Air flow	MiniAir64	Measuring Range: $0 - 40m/s$ Accuracy: 1%
Chamber	EPS	Dimensions 355mm x 265 mm x 545 mm Thermal Conductivity 0.035 W/mK Wall thickness 45mm
Pipes	Ventilation pipes	Material: Plastic
Fan	K 100 M Circular duct Fan	Air Transpose Capability: $0.051m^3/s$ AC 0-230 V
Speed Control	SEN-EVS-0-X-DT	
System Control	CompactRIO 9074	400 MHz processor 128 MB RAM 2 Ethernet and RS232 FPGA Spartan-3 2M

Table 4.2: Equipment

B. This procedure is continuously repeated until the system reach the steady state. An outline of the calculation process is shown in Figure 4.13.

The "heart" of this process is a script which calculated the final power losses. It is an embedded Matlab script serially running with the whole algorithm. It is responsible for indexing values of air properties from the arrays. Then, by linear interpolating these values the current values are calculated depending on the temperature variation. Air properties, heat capacity and density, presented in Table 4.1, are stored in arrays in the running algorithm at the initialization segment. In addition to this process, the wall losses are simultaneously calculated and then the final result is produced. Extended analysis of wall losses calculation will be presented in Subsection 4.7.1.

After that, there is a sampling process which samples the output value every 3.4 seconds. These values are stored in an array and a graph is also produced which is the characteristic curve of the system. Figure 4.14 illustrates a whole measurement graph where the steady-state is reacted after the 800^{th} sample.

4.7 Accuracy

The last but not least step is to take under consideration the accuracy of the implemented system. A main error contributor factor is the wall losses mentioned in the Subsection 4.4.3. After that, it is possible to calculate the overall error regarding the wall losses as a function of the temperature, chamber and ambient.

4.7.1 Wall Losses

The wall losses are calculated through Equations 4.6 and 4.7. The wall thickness d is equal to *0.048 meters* and the thermal conductivity equals $0.035W/mK$. The inner dimensions of the chamber is *0.355* x *0.265* x *0.545 m* which leads

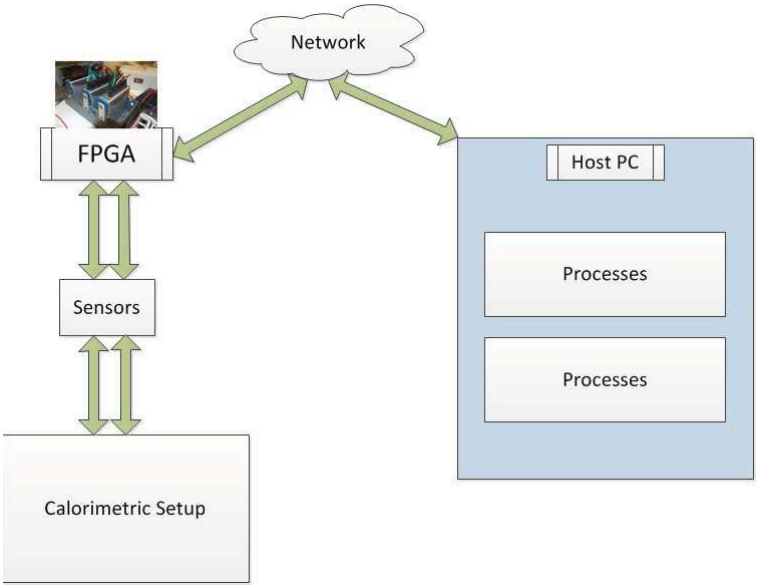

Figure 4.12: FPGA - host computer communication diagram

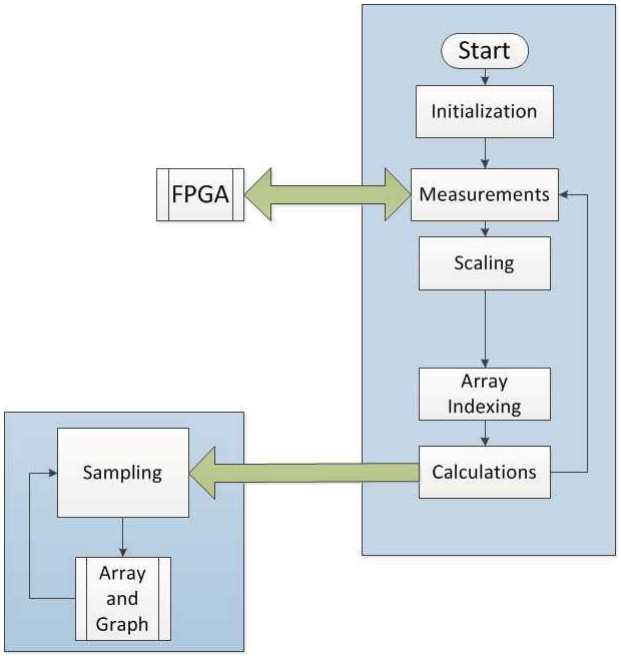

Figure 4.13: Block diagram of the measurement algorithm

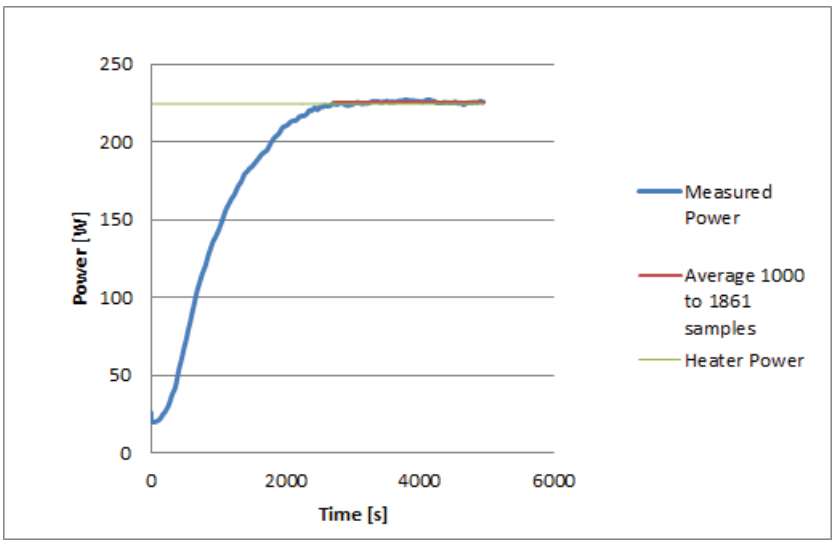

Figure 4.14: Measurement graph representing a full measurement process, indicating thermal steady state after 800 samples

to an inner area equals $0.76325\ m^2$. The thermal resistance is calculated as shown in the following Equation 4.9:

$$R_{th} = \frac{d_{wall}}{\lambda A_{wall}} = \frac{0.048}{0.035 \cdot 0.76325} = 1.79683^{o}C/W \tag{4.9}$$

The final wall losses are given by Equation 4.10 :

$$P_{wall} = \frac{T_{Chamber} - T_{Ambient}}{R_{th,wall}} = \frac{T_{Chamber} - T_1}{1.79683^{o}C/W} \tag{4.10}$$

where $T_{Ambient}$ is equal to inlet temperature T_1 and $T_{Chamber}$ is equal to the outlet temperature T_2 .

After calculating the wall losses the final calculation formula is changing to

$$P_{loss} = P_{cal} + P_{wall} \tag{4.11}$$

$$P_{loss} = \dot{V} \cdot \rho \cdot c_p \cdot (T_2 - T_1) + \frac{T_{Chamber} - T_1}{1.79683^{o}C/W} \tag{4.12}$$

which takes under consideration the whole energy dissipated from the DUT and the measurement is more precise and closer to the desired.

4.7.2 Overall Error

According to Equation 4.12 , P_{loss} is a function of $\dot{V}, T_2, T_1$. Assuming that $Z = P_{loss}$, then $\overline{X} = \dot{V}$,$\overline{Y} = T_2$ and $\overline{W} = T_1$. Applying Equation 3.17 in the function $P_{loss} = f(\dot{V}, T_2, T_1)$ the variance is calculated as shown in Equation 4.13. In order to simplify the calculations the specific heat capacity (both for inlet and outlet air) is considered to be constant and equal to each other.

$$\begin{aligned}\sigma_Z^2 = &[\rho_{T_1} \cdot c_{p_1} \cdot (T_2 - T_1)]^2 \cdot \frac{\sigma_{\dot{V}}^2}{n_{\dot{V}}} \\ &+ \left[\dot{V} \cdot \rho_{T_1} \cdot c_{p_1} + \frac{1}{R_{th_{wall}}}\right]^2 \cdot \frac{\sigma_{T_2}^2}{n_{T_2}} \\ &+ \left[-\dot{V} \cdot c_{p_1} \cdot \rho_{T_1} + \rho'_{T_1} \cdot \dot{V} \cdot c_{p_1} \cdot (T_2 - T_1) - \frac{1}{R_{th_{wall}}}\right]^2 \cdot \frac{\sigma_{T_1}^2}{n_{T_1}}\end{aligned} \tag{4.13}$$

Afterwards, the *variance of* T_1 is equal to the *variance of* T_2 because the measurement instruments are exactly the same. Then the samples n are also equal to each other as shown in the implementation in Section 4.6. Applying the following:

- $\sigma_{T_2}^2 = \sigma_{T_2}^2 = \sigma_T^2$
- $n_{T_2} = n_{T_1} = n_T$

Equation 4.14 shows the final variance calculation formula:

$$\begin{aligned}\sigma_Z^2 = &\left[\rho_{T_1} \cdot c_{p_1} \cdot (T_2 - T_1)\right]^2 \cdot \frac{\sigma_{\dot{V}}^2}{n_{\dot{V}}} \\ &+ \left[\dot{V} \cdot \rho_{T_1} \cdot c_{p_1} + \frac{1}{R_{th_{wall}}}\right]^2 \cdot \frac{\sigma_T^2}{n_T} \\ &+ \left[-\dot{V} \cdot c_{p_1} \cdot \rho_{T_1} + \rho'_{T_1} \cdot \dot{V} \cdot c_{p_1} \cdot (T_2 - T_1) - \frac{1}{R_{th_{wall}}}\right]^2 \cdot \frac{\sigma_T^2}{n_T}\end{aligned} \tag{4.14}$$

By replacing every component in Equation 4.14 with the following known values the final theoretical error calculation formula is given by Equation 4.15.

- $\rho'_{T_1} = -0.073\ kg/(m^3 \cdot K)$
- $\sigma_T^2 = 0.02^o C$
- $\sigma_{\dot{V}}^2 = 0.01 \cdot \dot{V}$

$$\begin{aligned}\sigma_Z^2 = &\left[\rho_{T_1} \cdot c_{p_1} \cdot (T_2 - T_1)\right]^2 \cdot \frac{(0.01 \cdot \dot{V})^2}{n_{\dot{V}}} \\ &+ \left[\dot{V} \cdot \rho_{T_1} \cdot c_{p_1} + \frac{1}{1.79683}\right]^2 \cdot \frac{0.0004}{n_T} \\ &+ \left[-\dot{V} \cdot c_{p_1} \cdot \rho_{T_1} - 0.073 \cdot \dot{V} \cdot c_{p_1} \cdot (T_2 - T_1) - \frac{1}{1.79683}\right]^2 \cdot \frac{0.0004}{n_T}\end{aligned} \tag{4.15}$$

To finish with, the averaging of the temperature and air flow values is set at 1000 samples. The theoretical error is calculated versus the power loss as shown in figure 4.15. As depicted, the error is decreasing as the power loss is increasing. Measurements from 0 W to 50 W may contain a much higher error compared to space from 50 W to 300 W.

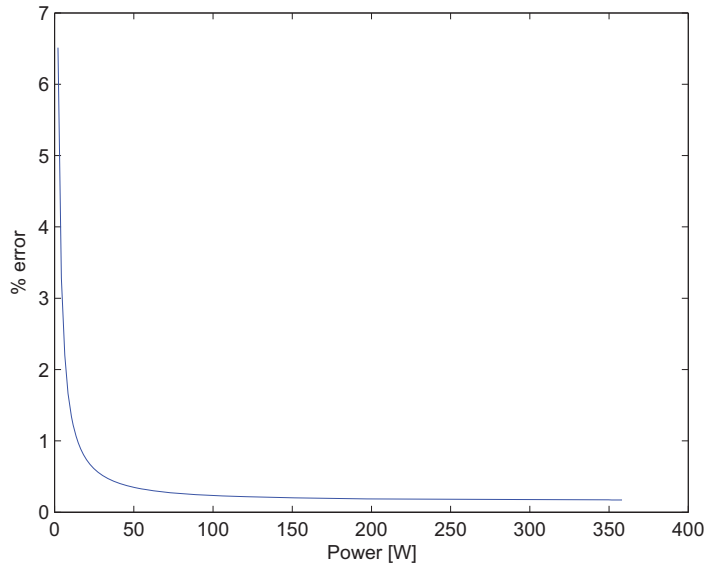

Figure 4.15: Theoretical error versus the power loss measurement

Chapter 5

Measurements

A variety of measurements were performed after the design and implementation of the calorimetric setup. First of all, it is necessary to calibrate the system. Then, measurements on a 6 kW dc/dc boost converter consisting of four parallel-connected SiC BJTs were performed. A short description of the converter along with various experimental results are shown.

5.1 Calibration process

According to Subsection 3.4 there are three kind of errors, from which the *Systematic errors* show up repeatedly. It is, therefore, possible to avoid them as they are repeated in every measurement and they also have the same impact. The idea of calibration is based on avoiding systematic errors. A heater power was placed in the measurement chamber as shown in Figure 5.1. It consists of four 10 Ω resistors which are connected in parallel and they are able to supply a power up to 400 W. A picture of the complete setup is shown in Figure 5.2. Several measurements were made starting from 25 W up to 300 W with a step of 25 W. The results are summarized in Table 5.1. It is remarkable that the percent error is decreasing as the measured power is increasing. Especially, for measured powers higher than 50 W the error is less than 7% while in the measuring range from 150 W to 300 W the accuracy reaches 1% or even better. These results are clearly presented in Figures 5.3 and 5.4. In Figure 5.3, the measured power versus the heater dc power is depicted where the red line represents the expected measured value versus the heater dc power. The deviation of this curve is the error of the calorimeter. This error is presented in Figure 5.4 where the percent error versus the heater dc power is shown.

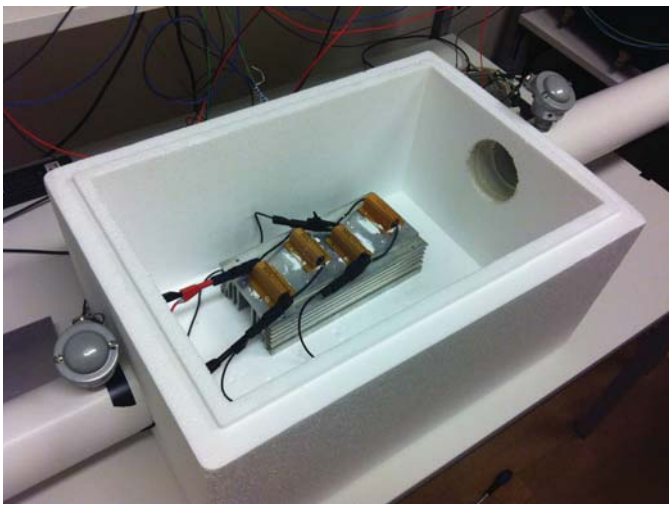

Figure 5.1: The heater power placed in the chamber. It consists of four 10 Ω resistors connected in parallel.

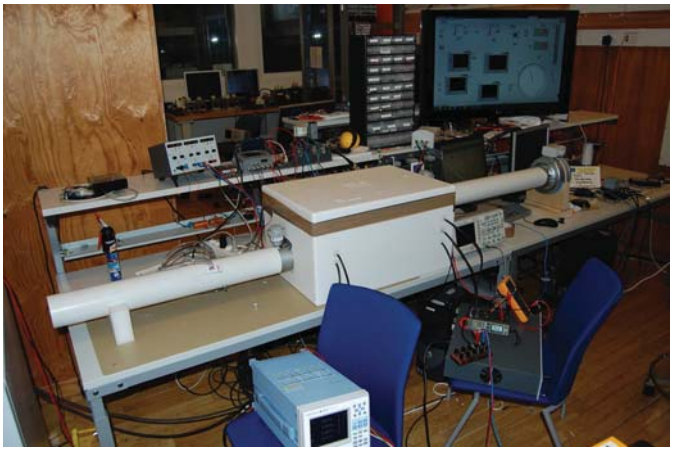

Figure 5.2: The Calorimetric setup during the measurements.

DC Power [W]	Measured Power [W]	Error [%]
25.22	20.83	17.43
51.78	48.21	6.89
75.94	72.85	4.07
102.47	99.93	2.48
124.39	122.13	1.81
152.40	150.76	1.08
174.51	173.81	0.40
201.77	201.28	0.24
224.44	224.20	0.10
251.34	251.10	0.09
275.62	275.55	0.02
309.05	308.89	0.05

Table 5.1: Calibration results of the calorimetric setup.

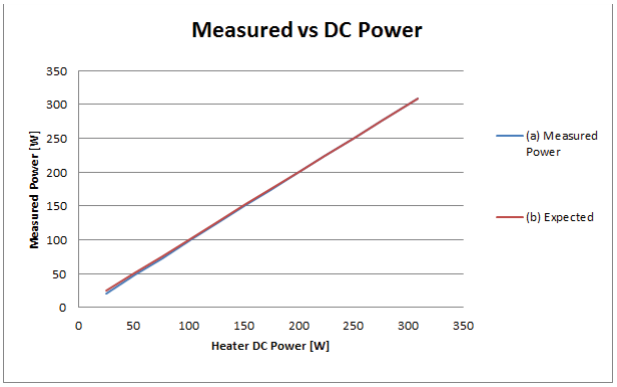

Figure 5.3: (a) Measured power versus heater dc power (blue line) (b) Expected measurement (red line)

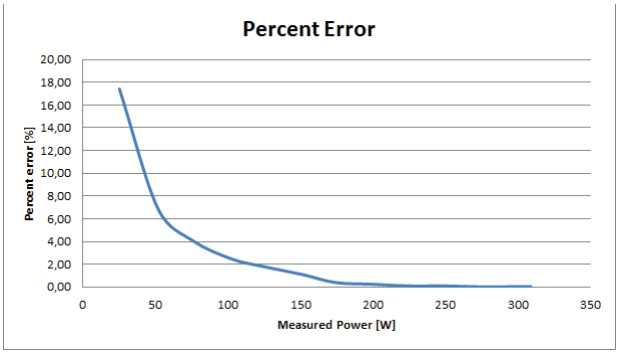

Figure 5.4: Percent error versus the final power measurement

5.2 Measurements of the SiC dc/dc Converter

Description of the converter

The dc/dc boost converter [39] is rated at 6 kW and operates at an input and output voltages of 300 V and 600 V, respectively (Figure 5.5). As shown in the schematic diagram of Figure 5.6 there are four parallel-connected SiC bipolar transistors (BJTs) in order to reach the desired power level. The converter has been designed to be able to operate either at 200 kHz or 250 kHz. The ratings of the converter have been chosen according to the current and voltage ratings of the BJTs (1200 V/ 6 A). Assuming that the desired power is 6 kW and a dc input voltage of 300 V, the input current equals 20 A. Moreover, the duty ratio has been set to 50%, so that the desired output voltage of 600 V is reached. Therefore, the output current is equal to 10 A. A primary design constraint of the converter deals with the compactness of the system. Special attention has been paid to this during the design and dimensioning phase. The dimensions of the converter are 175x100x90 mm and the volume equals 1.5 dm^3. The basic parameters of the converter are summarized in Table 5.2.

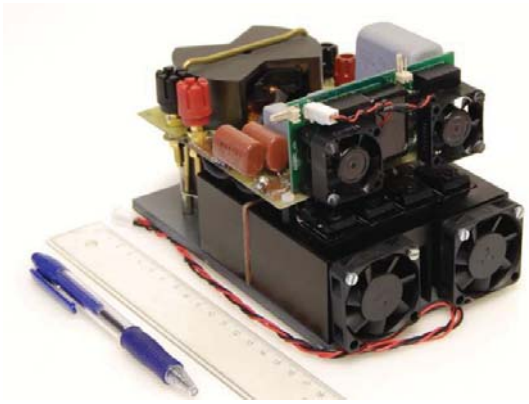

Figure 5.5: The 6 kW dc/dc boost converter

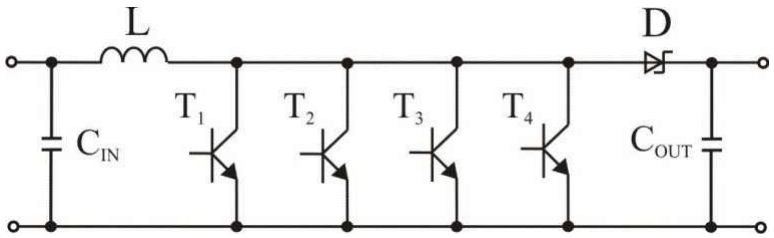

Figure 5.6: The schematic of the converter

Measurements

The converter was placed in the chamber as shown in Figure 5.7. Moreover, the microprocessor who is responsible for the device control was also placed inside the chamber. Power cables for the input and output voltage and current were mounted through the walls of the chamber. In the left side of the Figure 5.7 the inlet power wires are shown while in the right side the corresponding outlet. The chamber was shielded in order to avoid air and thermal leakage.

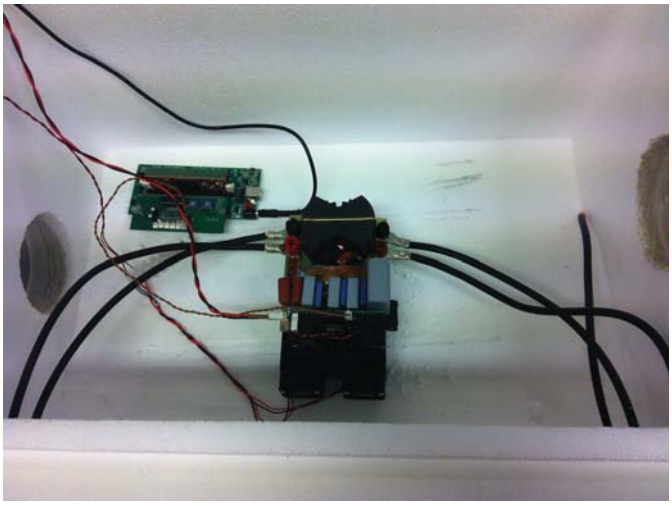

Figure 5.7: The converter inside the chamber

Various measurements were performed. The duration of each single measurement was approximately one hour and twenty minutes (1h 20min). The experimental verification was performed at 4 kW and 6 kW of output powers with a resistive load. Taking into account the two possible switching frequencies (250 kHz and 200 kHz) four measurement results are presented in total.

The first measurement was made at 6 kW and 250 kHz. The duration of the

Input voltage / current	300 V/ 20 A
Output voltage / current	600 V/ 10 A
Switching frequency	200 / 250 kHz
Duty Cycle	50%
Transistor	4xBiTSiC1206 (1200 V/ 6 A)
Diode	SiC Schottky SDP10S120D, (2x10A/1200V)
Inductor	$150\mu H/25A$
Input Capacitors	2x4.7 $\mu F/450V$
Output Capacitors	3x4.7 $\mu F/1kV$ 3x3 $\mu F/700V$ 1x20 $\mu F/700V$
Dimensions	175x100x90 mm, 1.5 dm^3

Table 5.2: Parameters of the dc/dc converter

Switching frequency [kHz]	**Inlet DC Power [W]**	**Outlet DC Power [W]**	**Power Losses Calorimeter [W]**	**Efficiency [%]**
250	6190.60	6057.30	106.28	98.283
250	4071.00	4007.80	62.09	98.475
200	6096.40	6011.10	88.88	98.542
200	4061.60	4061.60	49.64	98.778

Table 5.3: Power losses and efficiency measured results using the calorimetric setup

measurement was 1 hour and 20 minutes. In Figure 5.8(a) power versus time is shown. The red line represents the average of measured power for the last 20 minutes (400 samples) which give a reliable result. The final power losses are equal to 106.28 W.

Then, second set of measurements were performed. The total duration was one hour and twenty seven minutes (1h 27min). The results are shown in Figure 5.8(b). As for the previous measurement the result was an average of the last 20 minutes(400 samples). The power losses have been measured to be 62.09 W.

Afterwards, the setup was configured at 6 kW and 200 kHz. After one hour and twenty five minutes (1h 25min) of the measurement process the resulting curve is illustrated in Figure 5.8(c). By averaging the results obtained the the last 20 minutes the final power losses estimation is 88.88 W.

Finally, the last measurement was made at 4 kW and 200kHz. The duration of the measurement was also 1 hour and 17 minutes. The average power losses of the last 20 minutes equals 49.64 W. The outcome of the measurement process is shown in Figure 5.8(d)

The measurement results are summarized in Table 5.3. During the calorimetric measurements a power meter (Yokogawa WT500) was also used in order to simultaneously measure the power losses (indirect method). The calorimeter is able to measure the total power losses of the converter including the base driver and the cooling fan losses. However, the power analyzer only measures the power circuit losses. The power consumption of the base driver circuit and the cooling fans have been calculated in [39]. The power consumption of base driver are 7.5 W and the corresponding of the cooling fans are almost 5 W. The final power losses measured by the indirect method is shown at the 4^{th} column of Table 5.5. In Subsection 5.2 there is a full discussion and comparison of the results.

From the experiments, it has been shown that the time constant[1] of the system approximately equals to 11 minutes and 21 seconds (200 samples). This value was calculated considering the rising of the power from 0 W to its final value.

[1]The time constant τ was calculated according to the equation $P(t) = Pmax(1 - \exp(-t/\tau))$

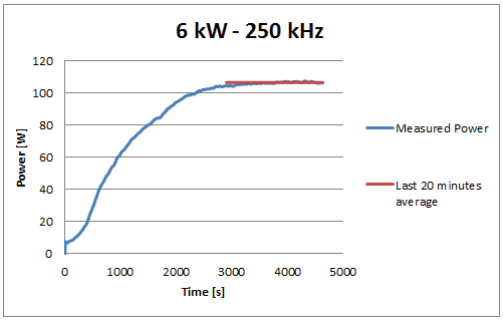

(a) 6 kW, 250kHz

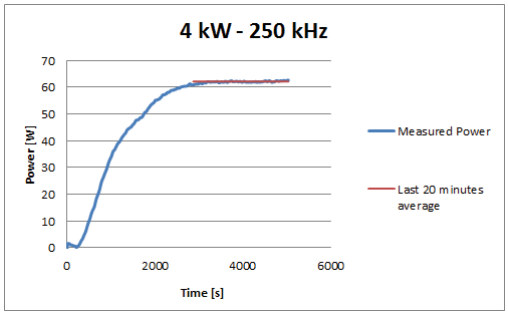

(b) 4 kW, 250kHz

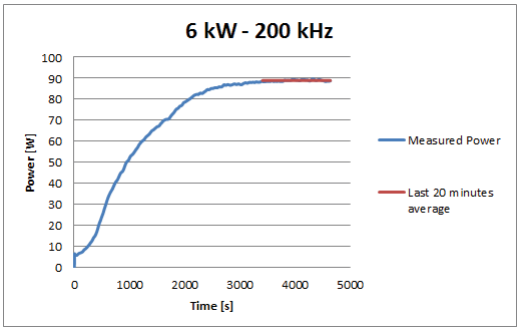

(c) 6 kW, 200kHz

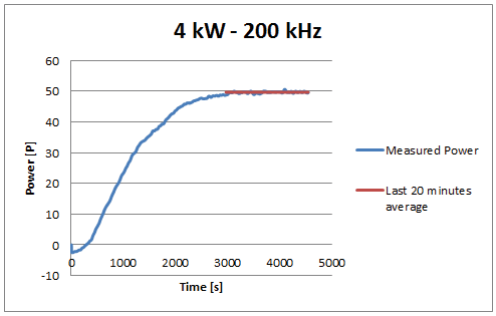

(d) 4 kW, 200kHz

Figure 5.8: Calorimetric measurement results

Switching frequency [kHz]	**Inlet DC Power [W]**	**Outlet DC Power [W]**	**Power Losses El. Method $P_{in} - P_{out}$ [W]**	**Efficiency [%]**
250	6190.60	6057.30	133.30	97.847
250	4071.00	4007.80	63.20	98.447
200	6096.40	6011.10	85.30	98.602
200	4061.60	4061.60	55.50	98.632

Table 5.4: Power losses and efficiency measured results using the power analyzer.

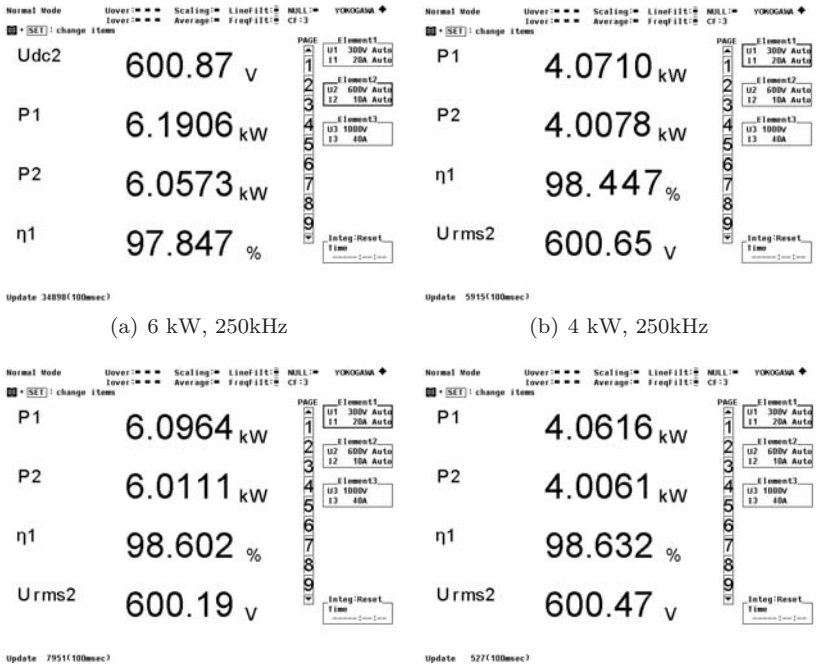

(a) 6 kW, 250kHz

(b) 4 kW, 250kHz

(c) 6 kW, 200kHz

(d) 4 kW, 200kHz

Figure 5.9: Screenshot of the Power Analyzer

Switching frequency [kHz]	Power [kW]	Power Losses Power Analyzer [W]	Power Losses plus Auxiliary [W]	Power Losses Calotimeter [W]	Deviation [%]
250	6	133.30	145.80	106.28	37.18
250	4	63.20	75.70	62.09	21.92
200	6	85.30	97.80	88.88	10.04
200	4	55.50	68.00	49.64	36.99

Table 5.5: Comparison of the measurement methods

Comparison of direct and indirect methods

According to the manufacturer, the accuracy of the power analyzer for power measurement is 0.2% which means 12 W and 8 W of errors at 6 kW and 4 kW respectively. This error is high compared to the power losses. For example, the error of 8 W is the 15% of the 55 W of power losses at 4 kW (200 kHz). This deviation[2] was also shown from the the comparison of the power losses results shown in Table 5.5.

As shown from Table 5.5 the deviation of the two methods is extremely high. It starts from 10% and may exceed 37%. Based on the theoretical background on direct and indirect loss measurements given in Chapter 3, it is believed that more accurate results are obtained using the calorimeter. The power losses caused in the converter are directly measured by means of temperature rise of air. Thus, measurement equipment, such as power meters, which introduce errors during voltage and current measurements are avoided. Furthermore, the calorimetric setup is able to measure power losses for the whole system. These power losses contain switching, conduction, magnetic, bus bars, cooling fans, cable and base driver power losses. Consequently, the efficiency of the whole system (converter) can be measured taking into account all the possible contributions of power losses. In Figure 5.10 there is an overview of different implemented calorimeters and their accuracies. It is also included the current setup highlighted with a light yellow spot and a corresponding accuracy.

Advantages of the Calorimeter

Based on the theoretical background given in this thesis along with the experimental results, the advantages of the calorimetric power loss measurement are itemized as follows:

- Using a calorimeter, the power loss measurement is not influenced by various voltage drops across, for instance, the supply cables, connection cables etc.

- The calibration of the calorimetric measurement system can be performed without the requirement of special instrumentation. However, the power of the heater used for the calibration must be accurately measured. This might introduce an error.

[2]Calculation formula: $\frac{P_{PowerAnalyzer}-P_{Calorimeter}}{P_{Calorimeter}} \cdot 100\%$

- Errors associated with voltage-current phase measurement are avoided. This kind of errors are usually introduced when power meters are used for efficiency measurements.

Disadvantages of the Calorimeter

On the other hand, the disadvantages of the calorimeter are itemized below:

- An adequately accurate measurement is obtained when the colorimetric system has reached the steady-state operation. This also implies that the operating point of the device which is measured must be constant. If, for instance, the device is facing a transient, an accurate measurement of the power losses will only be obtained when the steady-state is reached.
- The duration of each complete measurement process is longer than one hour which counts as a drawback for repeatable measurements.
- There are no commercially-available calorimeters. However, a customized design of a calorimeter should be made for each specific application.

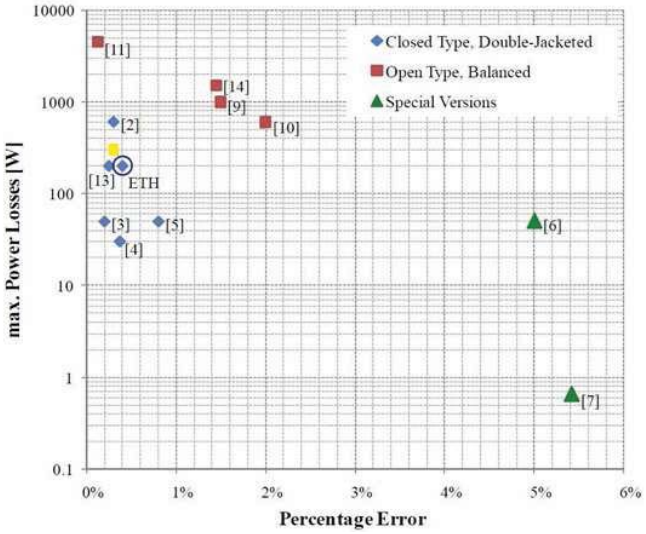

Figure 5.10: Overview of different implemented calorimeters and their accuracies including the current project highlighted with a light yellow spot. This figure was taken from [3]. The references of this figure correspond at the references of the source.

Chapter 6

Conclusion

The summary of this thesis is outlined in the following chapter. Future work guidelines and ideas for further improvement of the present work are given.

6.1 Summary

In this thesis the design process and the implementation of an open type calorimetric setup have been shown. At first, problems related to accurately measure the power losses of a converter were identified along with an overview of SiC semiconductors. Moreover, the theoretical background of calorimetry was given and a literature review of calorimetric setups was also discussed. The dimensioning of the system and the selection of the required equipment were presented in details. A presentation of the implementation procedure as well as the error calculation was also given. Finally, after the calibration process of the system several measurements were performed and the results are extensively discussed.

6.2 Main Results

The most significant results of this work are itemized as follows:

- It is possible to measure high efficiency SiC converters with high accuracy using calorimetric setups.
- Calorimetric setups are more accurate measurement techniques than the corresponding electrical methods.
- Open type calorimeters cost less than closed type calorimeters.
- Power loss measurements under 50 W are not accurate enough.

6.3 Future Work

The present thesis covers several aspects regarding measurement issues about SiC converters with high efficiency and high switching frequency. However, a

few important issues have been either simplified or neglected. A few issues which might be investigated in the future are outlined below:

- Extension of the concept for calibration to calorimeters with other sizes.
- Further investigation for power loss measurements under 50 W.
- Extension of the concept for calibration to closed-type calorimeters with water cooling.
- Implementation of automated calibration procedures.
- Further investigation of time constant and prediction of measurement in order to decrease the measurement time.
- Additional EMI shielding of the chamber using copper plates.
- Investigation of possible redundancy of the system.
- Optimization of the airflow distribution inside the chamber.
- Further investigation of wall power leakage regarding the calculations.

Bibliography

[1] J. Rabkowski, D. Peftitsis, and H.-P. Nee, "Silicon carbide power transistors: A new era in power electronics is initiated," *Industrial Electronics Magazine, IEEE*, vol. 6, no. 2, pp. 17–26, 2012.

[2] C. Xiao, G. Chen, and W. Odendaal, "Overview of power loss measurement techniques in power electronics systems," in *Industry Applications Conference, 2002. 37th IAS Annual Meeting. Conference Record of the*, vol. 2, oct. 2002, pp. 1352 –1359 vol.2.

[3] D. Christen, U. Badstuebner, J. Biela, and J. Kolar, "Calorimetric power loss measurement for highly efficient converters," in *Power Electronics Conference (IPEC), 2010 International*, june 2010, pp. 1438 –1445.

[4] J. Rabkowski, D. Peftitsis, and H.-P. Nee, "Design steps towards a 40-kva sic inverter with an efficiency exceeding 99.5%," in *Applied Power Electronics Conference and Exposition (APEC), 2012 Twenty-Seventh Annual IEEE*, feb. 2012, pp. 1536 –1543.

[5] V. Mattsson, "Comparison of calorimetric and electrical loss measurement methods in a frequency converter research and development application," in *Energy Conversion Congress and Exposition (ECCE), 2011 IEEE*, sept. 2011, pp. 1026 –1030.

[6] M. B. F.Keith, *Principles of Heat Transfer*. PWS Publishing Company, 1997, vol. 5th.

[7] M. Becker, *Heat Transfer: A Modern Approach*. Basic Books, 1986.

[8] A. Chapman, *Fundamentals of heat transfer*. Macmillan, 1987.

[9] B.Palm, *Short notes on Heat Transfer*. Department of Energy Technology, 1998, vol. 5th.

[10] R. Street, G. Watters, and J. Vennard, *Elementary Fluid Mechanics*. John Wiley & Sons, 1995.

[11] R. Sabersky, *Fluid flow: a first course in fluid mechanics*. Prentice Hall, 1999.

[12] P. Gresho and R. Sani, *Incompressible Flow and the Finite Element Method, Advection-Diffusion and Isothermal Laminar Flow*, ser. Incompressible Flow and the Finite Element Method. John Wiley & Sons, 2000.

[13] B. Mohammadi and O. Pironneau, *Analysis of the K-epsilon turbulence model*, ser. Recherches en mathématiques appliquées. Wiley, 1994.

[14] F. P. Incropera and D. P. DeWitt, *Fundementals of Heat and Mass Transfer*. Wiley, 2012.

[15] A. Agarwal, "An overview of sic power devices," in *Power, Control and Embedded Systems (ICPCES), 2010 International Conference on*, 2010, pp. 1–4.

[16] P. Friedrichs and R. Rupp, "Silicon carbide power devices - current developments and potential applications," in *Power Electronics and Applications, 2005 European Conference on*, 2005, pp. 11 pp.–P.11.

[17] A. Lindgren and M. Domeij, "1200v 6a sic bjts with very low vcesat and fast switching," in *Integrated Power Electronics Systems (CIPS), 2010 6th International Conference on*, 2010, pp. 1–5.

[18] A. Ritenour, D. Sheridan, V. Bondarenko, and J. Casady, "Saturation current improvement in 1200 v normally-off sic vjfets using non-uniform channel doping," in *Power Semiconductor Devices IC's (ISPSD), 2010 22nd International Symposium on*, 2010, pp. 361–364.

[19] J. Cooper, J.A., M. Melloch, R. Singh, A. Agarwal, and J. Palmour, "Status and prospects for sic power mosfets," *Electron Devices, IEEE Transactions on*, vol. 49, no. 4, pp. 658–664, 2002.

[20] D. Stephani, "Status, prospects and commercialization of sic power devices," in *Device Research Conference, 2001*, 2001, pp. 14–.

[21] J. Biela, M. Schweizer, S. Waffler, and J. Kolar, "Sic versus si evaluation of potentials for performance improvement of inverter and dc dc converter systems by sic power semiconductors," *Industrial Electronics, IEEE Transactions on*, vol. 58, no. 7, pp. 2872–2882, 2011.

[22] T. Friedli, S. Round, D. Hassler, and J. Kolar, "Design and performance of a 200-khz all-sic jfet current dc-link back-to-back converter," *Industry Applications, IEEE Transactions on*, vol. 45, no. 5, pp. 1868–1878, 2009.

[23] R. Lai, F. Wang, P. Ning, D. Zhang, D. Jiang, R. Burgos, D. Boroyevich, K. Karimi, and V. Immanuel, "A high-power-density converter," *Industrial Electronics Magazine, IEEE*, vol. 4, no. 4, pp. 4–12, 2010.

[24] S. Manias, *Power electronics*. Symeon Aris, 2012.

[25] W. Cao, K. Bradley, I. French, J. Zhang, and H. Zhang, "A review of calorimetric application for accurate power loss measurement," in *Universities Power Engineering Conference, 2006. UPEC '06. Proceedings of the 41st International*, vol. 2, sept. 2006, pp. 550 –554.

[26] N. Theodorou, *Electrical Measurements*. S.Athanasopoulos and SIA O.E., 2000.

[27] S. Weier, M. Shafi, and R. McMahon, "Precision calorimetry for the accurate measurement of losses in power electronic devices," *Industry Applications, IEEE Transactions on*, vol. 46, no. 1, pp. 278 –284, jan.-feb. 2010.

[28] S. Weier, R. McMahon, and P. Malliband, "Calorimetry for power electronics," in *Universities Power Engineering Conference, 2006. UPEC '06. Proceedings of the 41st International*, vol. 2, sept. 2006, pp. 608 –612.

[29] G. Chen, C. Xiao, and W. Odendaal, "An apparatus for loss measurement of integrated power electronics modules: design and analysis," in *Industry Applications Conference, 2002. 37th IAS Annual Meeting. Conference Record of the*, vol. 1, oct. 2002, pp. 222 –226 vol.1.

[30] P. Wolfs and Q. Li, "Precision calorimetry for power loss measurement of a very low power maximum power point tracker," in *Power Engineering Conference, 2007. AUPEC 2007. Australasian Universities*, 2007, pp. 1–5.

[31] P. McLeod, K. Bradley, A. Ferrah, R. Magill, J. Clare, P. Wheeler, and P. Sewell, "High precision calorimetry for the measurement of the efficiency of induction motors," in *Industry Applications Conference, 1998. Thirty-Third IAS Annual Meeting. The 1998 IEEE*, vol. 1, 1998, pp. 304–311 vol.1.

[32] A. V. den Bossche, "Flow calorimeter for power electronic converters," in *Poceedings of the EPE Conference 2001 , p27-29*, vol. 1, 2001, pp. 27–29.

[33] W. Cao, K. Bradley, and A. Ferrah, "Development of a high-precision calorimeter for measuring power loss in electrical machines," *Instrumentation and Measurement, IEEE Transactions on*, vol. 58, no. 3, pp. 570–577, 2009.

[34] U. Badstuebner, J. Biela, and J. Kolar, "An optimized, 99phase-shift pwm dc-dc converter for data centers and telecom applications," in *Power Electronics Conference (IPEC), 2010 International*, 2010, pp. 626–634.

[35] D. R. Turner, K. J. Binns, B. N. Shamsadeen, and D. Warne, "Accurate measurement of induction motor losses using balance calorimeter," *Electric Power Applications, IEE Proceedings B*, vol. 138, no. 5, pp. 233–242, 1991.

[36] K. Bradley, A. Ferrah, R. Magill, J. Clare, P. Wheeler, and P. Sewell, "Improvements to precision measurement of stray load loss by calorimeter," in *Electrical Machines and Drives, 1999. Ninth International Conference on (Conf. Publ. No. 468)*, 1999, pp. 189–193.

[37] P. Malliband, D. R. H. Carter, B. Gordon, and R. McMAHON, "Design of a double-jacketed, closed type calorimeter for direct measurement of motor losses," in *Power Electronics and Variable Speed Drives, 1998. Seventh International Conference on (Conf. Publ. No. 456)*, 1998, pp. 212–217.

[38] D. Peftitsis, G. Tolstoy, A. Antonopoulos, J. Rabkowski, J.-K. Lim, M. Bakowski, L. A?ngquist, and H. Nee, "High-power modular multilevel converters with sic jfets," *Power Electronics, IEEE Transactions on*, vol. 27, no. 1, pp. 28 –36, jan. 2012.

[39] J. Rabkowski, D. Peftitsis, and H.-P. Nee, "A 6kw, 200khz boost converter with parallel-connected sic bipolar transistors," in *Applied Power Electronics Conference and Exposition (APEC), 2012 Twenty-Seventh Annual IEEE*, feb. 2012, pp. 1536 –1543.

Abbreviations

Symbol	Description
SiC	Silicon Carbide
DUT	Device Under Test
NI	National Instruments
cRIO	Compact Reconfigurable I/O
EMI	Electromagnetic Interference
JFET	Junction gate Field-Effect Transistor
BJT	Bipolar Junction Transistor
MOSFET	Metal-Oxide-Semiconductor Field-Effect Transistor
FPGA	Field-Programmable Gate Array
Si	Silicon
EPS	Expandable Polystyrene
AC	Alternating Current
DC	Direct Current

Appendix A

Matlab

```
clc
clear all

%Initialize.................

%———————————————————————————Constrains
% Permit Velocity 3 to 10 m/s
% Permit 9 Pa to 10000 Pa
% Max. temperature of transported air 70 oC   //fan

% ———————————————————— units of measurement
%  V -> m^3 / sec
% densiy -> kg/m^3
% Cp -> kJ/(kg * K)
% ? -> C or K , ?? is the same
% P -> kJ/sec ,kW/s


%Density parameters
N=19;
            %Celcious
T = [-150 -100 -50 0 20 40 60 80 100 150 200 300 400 500 750 ...
    1000 1500 2000 2500];
            %Density
den = [2.897 2.046 1.584 1.293 1.205 1.127 1.060 1.000 0.946 ...
    0.834 0.746 0.616 0.524 0.456 0.345 0.277 0.199 0.155 0.126];
               %Cp
Cp = [1.016 1.008 1.006 1.006 1.006 1.007 1.008 1.010 1.011 ...
    1.017 1.025 1.045 1.069 1.093 1.144 1.193 1.282 1.468 2.200];


KL = 1;  %user manual debimo blades
r=0.1; %(m)


    Awall = 0.76325;
    Rth = 0.048/(Awall * 0.035);
    Pinit=0;



%————————————————————————————————————————————————————————————
```

```
%Variable Initializations
Ta=-1;
Tb=-1;
%Linear Interpolation
flag=1;
for i=1:N
    if (flag&((T(i)>T1) || (T(i)==T1)))
        Tb=T(i);
        a=i;
flag=0;
    end
end

flag=1;
for i=1:N
    if (flag&((T(N-i+1)<T1) || (T(N-i+1)==T1)))
        Ta=T(N-i+1);
        b = N-i+1;
flag=0;
    end
end

if (Ta ~= Tb)
denT1 = den(a)+(den(b)-den(a))*(T1-Ta)/(Tb-Ta);
CpT1 = Cp(a)+(Cp(b)-Cp(a))*(T1-Ta)/(Tb-Ta);
else
    denT1 = den(a);
    CpT1 = Cp(a);
end

%--T1  ...
    ------------------------------------------------------------------------

%-------------------------------------------------------------------------
%Variable Initializations
Ta=-1;
Tb=-1;
%Linear Interpolation
flag=1;
for i=1:N
    if (flag&((T(i)>T2) || (T(i)==T2)))
        Td=T(i);
        d=i;
flag=0;
end
end

flag=1;
for i=1:N
    if (flag&((T(N-i+1)<T2) || (T(N-i+1)==T2)))
        Tc=T(N-i+1);
        c= N-i+1;
flag=0;
    end
end

if (Tc~= Td)
denT2 = den(c)+(den(d)-den(c))*(T2-Tc)/(Td-Tc);
CpT2 = Cp(c)+(Cp(d)-Cp(c))*(T2-Tc)/(Td-Tc);
else
    denT2 = den(c);
    CpT2 = Cp(c);
```

```
101 end
102
103
104 %[denT1,a,b,CpT1] = LinIntDensity( T1 ); %Density for T1 (Linear ...
        Interpolation)
105
106 Pl=(10^3)* Q *(denT1*CpT1*(T2-T1));
107
108 Pwall=(T2 - T1)/Rth;
109
110 Plw= Pl + Pwall;
111
112
113 errorsmall = 100*(Psmall- Pdc)/ Pdc;
114 errorbig = 100* (Pbig- Pdc)/ Pdc;
115
116
117 %initialize error calc
118
119 dent2ton = -0.073;
120 nV=10000;
121 nT=1000;
122 sigmatetV = 0.05 * Q ;
123 sigmatetT = 0.2;
124
125 %error equation
126
127 sigmatetsmall = (denT1*1000*CpT1*(T2-T1)*sigmatetV)^2 / nV + ...
        (Q*denT1*1000*CpT1 + 1/Rth)*(sigmatetT)^2/nT + (-1/Rth ...
        -Q*denT1*1000*CpT1 + Q*1000*CpT1*(T2-T1)*dent2ton )^2 * ...
        (sigmatetT)^2 / nT;
128 ssSmall= (sigmatetsmall)^(0.5)
129 %============================================================
```

Appendix B

Labview

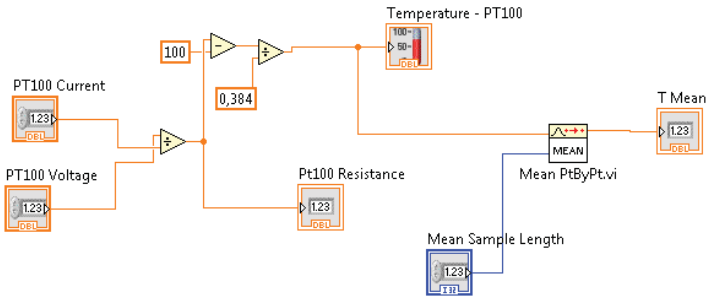

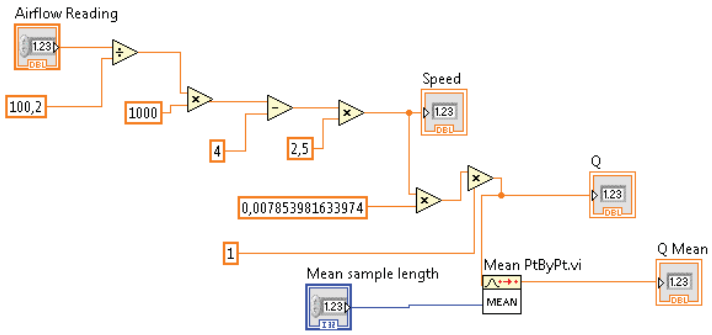

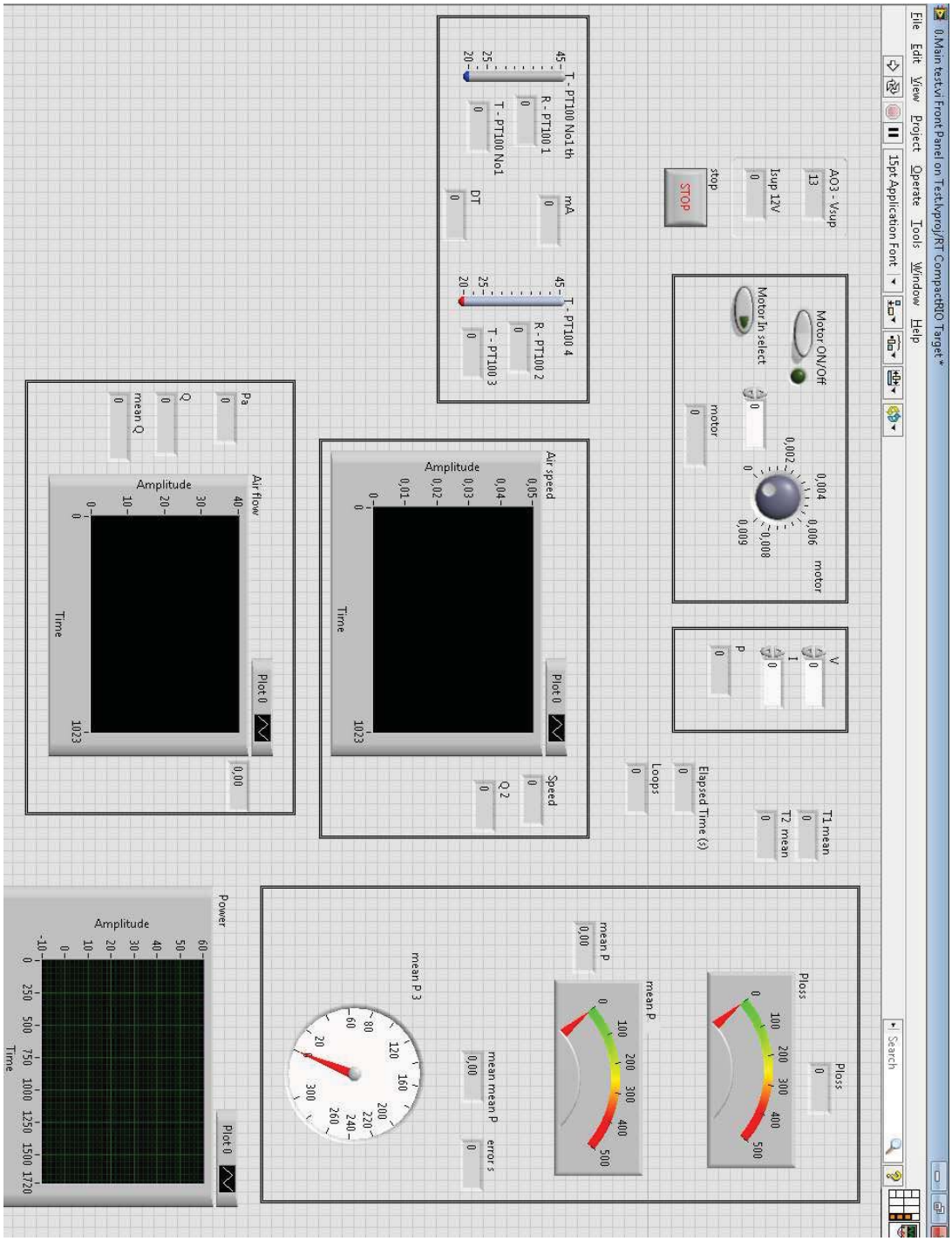
0.Main test.vi Front Panel on Test.lvproj/RT CompactRIO Target *
File Edit View Project Operate Tools Window Help
15pt Application Font
Search
AO3 - Vsup
13
Isup 12V
0
stop
STOP
Motor ON/Off
Motor In select
motor
0,002
0,004
0,006
0,008
0,009
motor
V
I
P
T - PT100 No1 th
R - PT100 1
T - PT100 No1
mA
DT
T - PT100 4
R - PT100 2
T - PT100 3
45
25
20
Air speed
Amplitude
Time
Plot 0
Speed
Q 2
Pa
Q
mean Q
Air flow
0,00
T1 mean
T2 mean
Elapsed Time (s)
Loops
Ploss
mean P
mean P 3
mean mean P
error s
Power
1023